Using multi-site data to apportion PM-bound metal(loid)s: Impact of a manganese alloy plant in an urban area

A. Hernández-Pellón, I. Fernández-Olmo

PII: S0048-9697(18)33711-2
DOI: doi:10.1016/j.scitotenv.2018.09.261
Reference: STOTEN 28765

To appear in: *Science of the Total Environment*

Received date: 11 July 2018
Revised date: 3 September 2018
Accepted date: 20 September 2018

Please cite this article as: A. Hernández-Pellón, I. Fernández-Olmo , Using multi-site data to apportion PM-bound metal(loid)s: Impact of a manganese alloy plant in an urban area. Stoten (2018), doi:10.1016/j.scitotenv.2018.09.261

Using multi-site data to apportion PM-bound metal(loid)s: Impact of a manganese alloy plant in an urban area

A. Hernández-Pellón[a*] and I. Fernández-Olmo[a]

[a] Dpto. de Ingenierías Química y Biomolecular, Universidad de Cantabria, Avda. Los Castros s/n, 39005 Santander, Cantabria, Spain

*Corresponding author
Dpto. de Ingenierías Química y Biomolecular, Universidad de Cantabria, Avda. Los Castros s/n, 39005 Santander, Cantabria, Spain
ana.hernandez@unican.es

Abstract

The identification and quantification of the PM emission sources influencing a specific area is vital to better assess the potential health effects related to the PM exposure of the local population. In this work, a multi-site PM_{10} sampling campaign was performed in seven sites located in the southern part of the Santander Bay (northern Spain), an urban area characterized by the proximity of some metal(loid) industrial sources (mainly a manganese alloy plant). The total content of V, Mn, Fe, Ni, Cu, Zn, As, Mo, Cd, Sb and Pb was determined by ICP-MS. This multi-site dataset was evaluated by positive matrix factorization (PMF) in order to identify the main anthropogenic metal(loid) sources impacting the studied area, and to quantify their contribution to the measured metal(loid) levels. The attribution of the sources was done by comparing the factor profiles obtained by the PMF analysis with representative profiles from known metal(loid) sources in the area, included in both the European database SPECIEUROPE (V2.0) and the US database EPA-SPECIATE (V4.5) or calculated from literature data. In addition, conditional bivariate probability functions (CBPF)s were used to assist in the identification of the sources. Four metal(loid) sources were identified: Fugitive and point source emissions from the manganese alloy plant (49.9% and 9.9%, respectively), non-exhaust traffic emissions (38.3%) and a minor source of mixed origin (1.8%). The PMF analysis was able to make a clear separation between two different sources from the manganese alloy plant, which represented almost 60 % of the total measured metal(loid) levels, more than 80% of these emissions being assigned to fugitive emissions. These results will be useful for the assessment of the health risk associated with PM_{10}-bound metal(loid) exposure and for the design of efficient abatement strategies in areas impacted by similar industries.

Keywords

Source apportionment, PMF 5.0, Multi-site data, Metal(loid)s, Manganese alloy plant

1. Introduction

Air pollution represents a major risk factor for human health (WHO, 2016a). Numerous epidemiological studies have related particulate matter (PM) exposure to a wide variety of cardiovascular and respiratory diseases (Fiordelisi et al., 2017; Lipfert, 2018) and neurodevelopmental and neurodegenerative disorders (Wang et al., 2017). Furthermore, PM from outdoor air pollution has been classified as carcinogenic to humans (Group 1) by the International Agency for Research on Cancer (IARC) (IARC, 2016).

PM toxicity is strongly influenced by the physico-chemical characteristics of particles (Kelly and Fussell, 2012), which may vary significantly due to the presence of different emission sources in urban, industrial and rural areas around the world (Mukherjee and Agrawal, 2017). In this regard, the identification and quantification of the emission sources influencing a specific area could be considered a suitable indicator of potential health effects of PM exposure (WHO, 2016b), being vital to design efficient abatement strategies, especially in areas impacted by local emission sources.

Different techniques have been applied to the identification and quantification of air pollution sources, namely emission inventories, source-oriented models (dispersion models), receptor models (RMs) and artificial neural networks (European Commission, 2013). Receptor and dispersion models are the most extensively used techniques for the quantification of source contributions in Europe (Fragkou et al., 2012). Whereas dispersion models account for transport, dilution and other processes taking place between source and receptor, RMs are less complex and are focused on the receptor site (European Commission, 2013).

The use of RMs has been extensively applied to the identification and apportionment of PM sources, using both, chemical composition (Agarwal et al., 2017; Alleman et al., 2010; Contini et al., 2012; Gregoris et al., 2016; Manousakas et al., 2017; Ramírez et

al., 2018; Viana et al., 2007; Zhang et al., 2018) and number size distribution (Friend et al., 2013; Leoni et al., 2018) as input datasets. Model inter-comparison was also used in a significant number of studies (Arruti et al., 2011; Belis et al., 2015; Bove et al., 2018; Cesari et al., 2016; Contini et al., 2016; Deng et al., 2018; Ogundele et al., 2016; Viana et al., 2008b), reporting strengths and limitations of the different approaches. Most frequent RMs are Chemical Mass Balance (CMB), Principal Component Analysis (PCA) and Positive Matrix Factorization (PMF) (Belis et al., 2013; Viana et al., 2008a; Watson et al., 2012). CMB requires the emission composition profiles for all relevant sources, whereas PCA and PMF are both based on a dataset of the measured species at the sampling sites. In this regard, the use of representative profiles included in both the European database SPECIEUROPE (V2.0) (Pernigotti et al., 2016) and the US database EPA-SPECIATE (V4.5) (U.S. Environmental Protection Agency EPA, 2016), is essential as input for models using the CMB approach, but also for verifying profiles in the PCA or PMF approach. However, as reported by Cesari et al. (2016), the lack of knowledge about the chemical profiles of site-specific sources could be a limitation when performing the CMB approach.

Although PCA was the most frequently used RM up to 2005 (Viana et al., 2008a), Belis et al. (2013) found a shift between these techniques towards models able to handle uncertainties on the input and output, such as PMF. The main advantage of this model is that it forces all of the values in the solution profiles and contributions to be nonnegative, which is more realistic than in PCA (Reff et al., 2007). In addition, several improvements have been included in the last version of this software, EPA PMF 5.0. Firstly, as demonstrated in Sofowote et al. (2015a) and Sofowote et al. (2015b), it is possible to establish mathematical constraints, based on known information, that guide the evolution of the factor solutions, allowing to reduce the rotational space. Secondly,

the uncertainty of the PMF solution can be evaluated by two additional error estimation methods, displacement (DISP) and bootstrapping with displacement (BS-DISP) described in detail in Paatero et al. (2014) and Brown et al. (2015). Moreover, EPA PMF 5.0 includes the ability to read multiple site data. This can be applied to samples collected simultaneously

(Cesari et al., 2016; Kara et al., 2015; Pandolfi et al., 2011), but also consecutively (Contini et al., 2012; Orogade et al., 2016; Owoade et al., 2015). The key receptor modeling assumption is that the composition of the sources impacting the sites does not change between sites (U.S. Environmental Protection Agency EPA, 2014). This approach has proven to increase the statistical significance of the analysis (Contini et al., 2016).

The combination of a source apportionment obtained from a RM approach with local wind direction data may be helpful to assist in the identification of specific sources (Hopke and Cohen, 2011). The relation between pollutant concentration and wind direction is usually reported by pollutant concentration roses or Conditional Probability Functions (CPFs) (Al-Harbi, 2014; Argyropoulos et al., 2017). Also, bivariate polar plots, which include wind speed as an additional variable, have been applied to source apportionment studies to obtain information about the dispersion of specific pollutants or sources (Di Gilio et al., 2017; Grange et al., 2016). A combined method termed Conditional Bivariate Probability Function (CBPF) has been recently used in source apportionment studies (Bari and Kindzierski, 2018; Mukherjee and Agrawal, 2018; Squizzato et al., 2017). CBPF can be applied considering intervals in the concentration of species, rather than only values greater than some threshold, thus, providing much more comprehensive information for source identification (Uria-Tellaetxe and Carslaw, 2014).

In this work, the levels of potentially toxic metal(loid)s (i.e. V, Mn, Fe, Ni, Cu, Zn, As, Mo, Cd, Sb and Pb) have been determined in PM_{10} samples collected in seven sites located in the southern part of the Santander Bay (northern Spain). This area, which is impacted by the same metal(loid) sources, is of especial interest due to the proximity of a manganese alloy plant to an urban area, where high levels of Mn, according to the World Health Organization (WHO) criteria, have been reported (Hernández-Pellón and Fernández Olmo, 2016; Moreno et al., 2011). Since metal(loid)s are good tracers of local industrial emissions (Querol et al., 2007), this multi-site dataset was evaluated by PMF in order to identify the main anthropogenic metal(loid) sources and to quantify the contribution of these sources to the measured metal(loid) levels in the studied area.

2. Materials and methods

2.1 Area of study

This study was conducted in the north of Spain, in the region of Cantabria (580,140 inhabitants, 2017), specifically in the southern part of the Santander Bay. This is an urban/industrial area mainly characterized by high Mn air concentrations (Moreno et al., 2011; Ruiz et al., 2014) according to the World Health Organization (WHO) criteria. The location of a manganese alloy plant in the area, which specializes in silicomanganese (SiMn) and ferromanganese (FeMn) production, has been previously identified as the main source of Mn (Moreno et al., 2011). To perform this study, seven monitoring sites were selected around the manganese alloy plant, distances ranging from 0.3 to 2.5 km, in order to contemplate the most frequent wind direction scenarios. The name, code, location and distance from the manganese alloy plant of the seven sites are shown in Table 1. Among the selected sampling locations, there are two official monitoring stations that belong to the Cantabrian Regional Government (CROS and

GUAR), one primary school (CPJH), three municipal centers (CULTJH, CCV and CMFC) and the garden of a private house (GUARCRC). The location of the sampling sites and manganese alloy plant is shown in Figure 1. Additionally, Figure 2 shows the wind roses calculated for the sampling periods at the seven monitoring sites. As can be seen, the most frequent winds came from the S-SW and NNE direction during the whole sampling campaign, in agreement with the prevailing wind directions of the region. Light winds blowing from the SW from midnight until mid-morning and NE onshore moderate sea breezes during the afternoon are usually found in the Cantabrian coastal area (Moreno et al., 2011), especially during the warm months of the year (see Figure 2).

2.2 Sampling and analysis

A PM_{10} sampling campaign was performed from January to December 2015, at the seven monitoring sites shown in Table 1 and Figure 1. PM_{10} samples were collected by means of a low volume sequential sampling device (2.3 m^3/h) equipped with a 15-filter cartridge, on 47 mm quartz fiber filters (Sartorius). The sampler was moved once a month to a different location in order to collect 28 daily samples per site and a total of 196 samples during the whole sampling campaign.

The total content of metal(loid)s in PM_{10} samples was determined based on the European standard method "EN-UNE 14902-2006". After gravimetric determination, the acid digestion of the filters was performed in a microwave digestion system (Milestone Ethos One) using closed Teflon vessels (HNO_3:H_2O_2 with a mixture of 8:2 ml, up to 220 ºC) and the total content of V, Mn, Fe, Ni, Cu, Zn, As, Mo, Cd, Sb and Pb was analyzed by inductively coupled plasma mass spectrometry (ICP-MS, Agilent 7500 CE). Quality control of the analytical procedure included the determination of the recovery values of the analyzed metal(loid)s from a standard reference material (NIST

SRM 1648a, "Urban particulate matter"), as well as the evaluation of the blank contribution from the filters and reagents and subsequent subtraction from the results. Recovery values and method detection limits (MDL) of the mentioned metal(loid)s are shown in Table 2.

2.3 Data analysis

The statistical analysis of the metal(loid) concentrations obtained at each sampling site was performed using R statistical software version 3.3.0. Due to the relatively small number of samples per location, the Shapiro-Wilks test was selected to check the normality of the data distributions. Since most distributions deviated from the normality, the relationship between metal(loid) concentrations at each studied site was evaluated by determining the Spearman correlation coefficients.

2.4 Source apportionment

The source apportionment analysis was performed using EPA PMF 5.0. PMF theoretical basis is explained in detail in Paatero et al. (2014). It is a multivariate factor analysis tool that apportions the measured mass of a pollutant at a given site to its emission sources, solving a mass balance equation (Eq.(1)):

$$x_{ij} = \sum_{k=1}^{p} g_{ik} f_{kj} + e_{ij} \qquad (1)$$

where x_{ij} is the concentration of each pollutant, p is the number of factors, f_{kj} the species profile of each source, g_{ik} the amount of mass contributed by each factor to each individual sample and e_{ij} the residual for each sample/species.

These factor contributions and profiles are derived by the PMF model minimizing the objective function Q (Eq.(2)), with the constraint that nonnegative values in the solution are allowed (Hopke, 2016):

$$Q = \sum_{i=1}^{n} \sum_{j=1}^{m} \left[\frac{x_{ij} - \sum_{k=1}^{p} g_{ik} f_{kj}}{u_{ij}} \right]^2 \qquad (2)$$

where u_{ij} is the uncertainty associated with the measurement of each pollutant concentration in each sample (U.S. Environmental Protection Agency EPA, 2014).

Table 3 summarizes the settings used for the PMF analysis. The multi-site dataset was composed of eleven metal(loid) concentrations (i.e. V, Mn, Fe, Ni, Cu, Zn, As, Mo, Cd, Sb and Pb) and the 196 samples collected at the seven monitoring sites were considered together in a single run. The sum of all the measured metal(loid) levels was provided as the total variable. A statistical study was conducted to detect the presence of outliers in the dataset. Different methods are reported in the literature for uncertainty calculation (Reff et al., 2007). In this study the uncertainties of metal(loid)s below the MDL were calculated as 5/6 MDL, whereas for data above the MDL the uncertainties were calculated following Eq.(3) (U.S. Environmental Protection Agency EPA, 2014).

$$u_{ij} = \sqrt{(EF \times x_{ij})^2 + (0.5 \times MDL)^2} \qquad (3)$$

where EF is the error fraction, which represents the potential error associated with the measurement of each metal(loid) concentration, including the error related to the sampling and to the analytical procedure.

Species were classified as “good”, “weak” or “bad” according to the signal to noise ratio (S/N) criteria reported in U.S. Environmental Protection Agency EPA (2014) and the percentage of samples above the MDL. Total variable was classified as weak by default. A total of 100 runs and a random seed were used to avoid the obtention of a local minima.

The best model was selected based on several criteria: (i) the ratio between Q_{robust} and $Q_{theoretical}$ (U.S. Environmental Protection Agency EPA, 2014), (ii) the comparison between predicted and observed data through the time series and the scaled residual

distributions, (iii) the significance test (p-value), (iv) the physical meaning of the factors, and (v) the evaluation of the error estimation diagnostics of the model (i.e. DISP, BS and BS-DISP methods). Fpeak values between -5 and 5 were explored in order to evaluate possible alternative solutions.

2.5 Conditional bivariate probability function (CBPF)

The conditional probability function (CPF) calculates the probability that in a particular wind sector the concentration of a species is greater than some specified value, this value usually being expressed as a high percentile of the species of interest (e.g. the 75th or 90th percentile) (Uria-Tellaetxe and Carslaw, 2014). The conditional bivariate probability function (CBPF) combines CPF with wind speed and it is defined as:

$$CBPF = \frac{m_{\theta_j}}{n_{\theta_j}}$$

where $m_{\theta j}$ is the number of samples in the wind sector θ and wind speed interval j greater than a specified value, and $n_{\theta j}$ is the total number of samples in the same wind direction-speed interval (Carslaw, 2015). CBPF analysis is very useful for showing which wind direction and speed intervals are dominated by high concentrations.

In this study, CBPF plots were applied to the source contributions obtained by PMF 5.0, using the R statistical software version 3.3.0 and the Openair package for air quality data (Carslaw and Ropkins, 2012). The 75th percentile of the factor contributions was established as the reference value for CBPF calculation. Hourly wind speed and direction were used as input data.

3. Results and discussion

3.1 Metal(loid) levels in the vicinity of a manganese alloy plant

The mean and standard deviation of the measured metal(loid) concentrations in PM_{10} at the studied locations are summarized in Table 4. The highest concentrations were found for Mn, Fe, Zn and Pb. These metals are frequently related to the manganese alloy industry (Mbengue et al., 2015; Marris et al., 2012). In addition, moderate, but lower concentrations were found for Cu, which is usually related, together with Fe and Zn, to non-exhaust road traffic emissions (Fomba et al., 2017). The difference in metal(loid) concentrations between the studied sites could be attributed to the different distances from the main anthropogenic sources, but also to the different meteorological conditions (i.e. wind direction and speed, and precipitation) and emission patterns during the sampling periods. For instance, although the CROS and CMFC sites are located very close, the sampling at the CMFC site coincided with a period of low rainfall (42 mm), while precipitation at the CROS site during the sampling period was much higher (300 mm), leading to higher metal(loid) concentrations at the CMFC site with respect to CROS, as observed in Table 4.

Although Mn is not included in EU air quality Directives, the World Health Organization (WHO) establishes an annual mean value of 150 ng/m^3 as a guideline. In this regard, these results suggest that Mn levels would exceed by far the WHO recommendation in six of the seven monitoring sites. This tendency was corroborated from a parallel extensive annual sampling campaign carried out at the CROS site in 2015 (one sample per week, 52 samples), where an annual mean Mn level of 231.8 ng/m^3 was obtained, similar to the monthly mean value reported in Table 4 (266.7 ng/m^3). Thus, and due to the relation established between Mn exposure and neurotoxic disorders (Chen et al., 2016), Mn is a metal of special concern in the studied area, especially in relation with its potential health effects on susceptible groups like children (Bjørklund et al., 2017).

3.2 Site-comparison of metal(loid) levels in the studied area

As Table 4 shows, the highest mean concentrations of most metal(loid)s were found at the CCV, CMFC and CPJH sites, located N-NW from the manganese alloy plant, in the direction of the plume coming from the plant when the prevailing winds of the region (S-SW) were blowing. Only As and Ni concentrations were higher on average at the GUAR site.

Spearman correlation coefficients between the analyzed metal(loid)s were evaluated in all of the sampling sites. Tables 5 and 6 present the correlations found between the metal(loid)s frequently related to the manganese alloy industry (i.e. Mn, Fe, Zn, Cd and Pb) (Marris et al., 2012) and to non-exhaust traffic emissions (i.e. Fe, Zn, Cu, Sb and Mo) (European Commission, 2014; Dongarrà et al., 2009; Sjödin et al., 2010), respectively. As Table 5 shows, strong or moderate correlations were found at the CROS and CCV sites between all metals frequently associated with the manganese alloy industry. As can be seen in Figure 3, this interdependence was also verified by the time series of Mn, Zn, Cd and Pb concentrations at the mentioned sites. This relation was also found to a lesser extent at the GUAR, CMFC or GUARCRC sites.

It should be noted that although Fe-Mn showed a strong correlation at the CROS and CCV sites, no other strong and significant correlation was found at the rest of the studied sites between these metals, which could indicate the influence of additional Fe sources in the area. As can be observed in Table 4, the highest Fe concentrations were measured at the CMFC and GUARCRC sites, both located less than 15 m from the railroad tracks. The lack of interdependence between Mn and Fe in some of the sampling sites located close to the manganese alloy plant could also be explained by the change in the production patterns of the plant from FeMn to SiMn during the sampling period. In this regard, according to Kero et al. (2015) and Gjønnes et al. (2011) the

presence of Fe in the dust from the SiMn smelting unit is negligible and the presence of Mn-Fe oxides is associated with the FeMn production.

As Table 6 shows, strong or moderate correlations were found between Fe, Cu, Sb and Mo in most of the studied sites. These metal(loid)s are frequently associated with non-exhaust traffic emissions (European Commission, 2014; Dongarrà et al., 2009; Sjödin et al., 2010). The strongest correlations ($r>0.8$, $p<0.01$) were reported at the CROS, GUAR and GUARCRC sites, all located close to medium or high traffic-urban areas. As can be seen in Figure 3, a similar pattern in the time series of Fe, Cu and Sb concentrations was found at the CROS, GUAR and GUARCRC sites. Although Mo seems to follow the same tendency at these locations, the large number of samples below the MDL hinders this comparison. In addition, as Table 6 shows, strong or moderate correlations were also found at the CCV and CPJH sites. At the CULTJH site, which is the site located further from the urban core, a high correlation coefficient was only found for Cu-Sb. In addition, as can be seen in Table 6, the correlation between Zn and other tracers of non-exhaust traffic emissions (i.e. Cu, Sb and Mo) is not clear in most sampling sites, which could suggest the influence of additional Zn sources in the area (e.g. the manganese alloy plant).

3.3 Metal(loid) source identification by PMF

A four-factor model was selected as the most stable solution. The following metal(loid) sources were identified: fugitive emissions from the manganese alloy plant (49.9%), non-exhaust traffic emissions (38.3%), point sources from the manganese alloy plant (9.9%) and a minor source of mixed origin (1.8%). Figures 4 and 5 show the source profiles and the contribution of each source per site, respectively.

Table 7 presents the summary of the PMF and error estimation diagnostics for the selected model. As can be seen, no swaps were found with DISP error analysis

(dQ^{max}<<1%), indicating the absence of significant rotational ambiguity and therefore the robustness of the solution (U.S. Environmental Protection Agency, 2014). Additionally, no unmapped factors were observed with BS error analysis (dQ^{max}<<1%) and the mapping was over 91% for the four factors, which suggest that the BS uncertainties can be interpreted and the number of factors may be appropriate (U.S. Environmental Protection Agency EPA, 2014). The use of different Fpeak values did not lead to a better interpretability of the factors, therefore the optimum solution was selected without any rotation (Fpeak = 0).

Details about the composition and attribution of the identified factors are presented below.

Fugitive and point sources from the manganese alloy plant. The factors related to the manganese alloy plant are jointly discussed. The relative composition of the factor associated with the fugitive emissions, which represented the 49.9% of the total measured metal(loid) concentrations, followed the order Mn>Fe>Zn>Pb, with more than 90% of the total Mn load associated with this factor. On the other hand, the relative composition of the factor related to the point sources, with a 9.9% of contribution to the total measured metal(loid) concentrations, followed the order Zn>Mn>Pb≈Fe>Cd. Both factors correspond to the two main groups of metal(loid) sources that can be distinguished during the manganese alloy manufacturing process. Firstly, in the smelting units, the off-gas exiting the electrical furnaces is cleaned by wet scrubbers and flared off, representing the main point source of the plant. In addition, dust from the tapping, ladle and casting operations is generated and hooded towards a baghouse before exiting through a chimney. As Figure 6a shows, despite the limitation that Mn and Fe is not included in the European Pollutant Release and Transfer Register (e-PRTR), the relative composition of the factor associated with the point sources is very

similar to the relative factor profile calculated from the emission data included in the e-PRTR in 2015 for the reported metal(loid)s. It should be noted that the company only reports in the e-PRTR the emission of metal(loid)s from point sources.

Secondly, unhooded dust generated in the tapping, ladle and casting operations is released through the openings located in the walls of the smelting buildings. Additionally, fugitive emissions can also originate from uncovered ore or slag piles. In this regard, as Figure 6(b,c) shows, there is a good agreement between the factor profile related to the fugitive emissions and the relative factor profiles calculated from baghouse PM_{10} samples collected in a manganese alloy plant, obtained from the EPA 4.5 SPECIATE database, and from samples collected in a mixing of raw materials area inside a manganese alloy plant in Norway, reported by Gunst et al. (2000). Therefore, this factor can be attributed to fugitive emissions from the smelting buildings (the chemical profile should be similar to that of the baghouse samples) and from the Mn ores. A previous study developed in the vicinity of the same manganese alloy plant, identified that 72% of the Mn emissions are from fugitive sources, 66% from the smelting buildings, whereas only 6% are from ore or slag piles (Otero-Pregigueiro et al., 2018). Carter et al. (2015) also reported that the fugitive emissions from a manganese alloy plant represents up to 65% of the total Mn emissions. The present study reveals that more than 80% of the studied metal emissions coming from the manganese alloy plant are attributed to fugitive emissions.

As can be seen in Figure 5, the sites where the factors related to the manganese alloy plant presented the highest contributions were CCV, CMFC and CPJH, which are located in the direction of the plume coming from the plant when the prevailing winds of the region are blowing (see Figure 2). Additionally, Figures 7 and 8 show the comparison of the CBPF plots for these factors at the closest sites from the manganese

alloy plant (i.e. CROS, GUAR, CCV and CPJH sites). As Figure 7 shows, the highest contributions of the fugitive and point source emissions at the sites where samples were collected during the cold season (i.e. CROS and GUAR sites) come from the S and N-NE direction, respectively, in accordance with the location of the manganese alloy plant with respect to these sites (see Figure 1). On the contrary, as can be seen in Figure 8, at the sites where samples were collected during the warm period and located N/NE of the plant (i.e. CCV and CPJH sites), the highest contributions of both factors pointed to the S-SW sector, but also to the NE sector, where no Mn sources are located. This fact can be explained by the changes from SW winds in the night and morning to NE sea breezes during the afternoon (Moreno et al., 2011). Under this scenario (i.e. warm period), the plume emanating from the manganese alloy plant typically moves NE during the night and morning reaching the CCV and CPJH sites, blowing back SW in diluted form by afternoon sea breezes. In this regard, the use of the CBPF approach in metal(loid) source identification studies presents limitations in relation with the changes in wind direction throughout the day, due to the low temporal resolution of the measured metal(loid) concentrations.

Figures 7 and 8 also show that the probabilities associated with the specific wind speed and directions where the major contributions of the point source emissions could be found, are generally lower than the probabilities found for the fugitive sources, with the exception of the CROS site. Since fugitive emissions are not released through a confined controlled airstream (i.e. chimneys), these emissions are expected to have less buoyancy (Fulk et al., 2016), and the probability of finding high contributions is higher at the closest receptor sites downwind of the source. On the other hand, point sources seem to be more influenced by changes in the wind direction, mainly in the warm

period, leading to lower probabilities of reaching high contributions at the closest locations from the plant.

Non-exhaust traffic emissions. This factor represented the 38.3% of the total measured metal(loid) concentrations and was mainly composed of Fe, Zn, Mn and Cu. Key tracers were Fe, Cu, Sb and Mo. All these metal(loid)s are associated with non-exhaust traffic emissions. Brake wear PM_{10} is characterized by the presence of high concentrations of Fe, Cu, Zn and Sb, whereas tyre wear PM_{10} is characterized by high concentrations of Zn, with lower amounts of Cu and Mn (European Commission, 2014). Whereas Fe, Zn, Cu and Sb are clearly associated with non-exhaust traffic emissions in the literature (European Commission, 2014; Dongarrà et al., 2009), the origin of Mo is attributed to the emission of exhaust gases, but also to brake and tyre wear (Sjödin et al., 2010). In addition, Mo can also be found in engine lubricants and incorporated into road dust through oil leakage (Spada et al., 2012).

This profile factor was compared with several urban traffic emission profiles found in the Specieurope database. Figure 6d shows the comparison between this profile factor and the factor profile from re-suspended PM_{10} urban road dust reported by Cesari et al. (2012). As Figure 5 shows, the sites where this factor presented the highest contributions were CROS, GUAR, CMFC and GUARCRC, all located next to medium or high traffic-urban areas and in the case of the CMFC and GUARCRC sites, also located very close to the railway tracks.

Mixed source. This factor, with a contribution of only 1.8% to the total measured metal(loid) concentrations, was mainly composed of Zn, Mn, Fe, V, Ni and As. Vanadium and Ni were considered the main tracers of this factor. These metal(loid)s are frequently associated with oil combustion processes, specifically with ship exhaust emissions (Popovicheva and Demirdjian, 2009; Streibel et al., 2017; Wu et al., 2017).

The Ni and V content in ship emissions is determined by the composition of fuel and lubricant oil (Moldanova et al., 2013). Ratios of V/Ni between 1-8 associated with ship exhaust emissions can be found in the literature (Viana et al., 2009; Moreno et al., 2010). In this regard, the high variability in V and Ni content in the common oils used as fuel by shipping (i.e. marine gas oil (MGO), HFO and diesel fuel (DF)) hinders the use of this ratio as tracer in source identification (Moreno et al., 2010). In this study, the V/Ni ratios ranged from 0.4 to 1.2, the highest being reported at the CULTJH and CCV sites, whereas the V/Ni ratio of the factor was 1.1. The low V/Ni ratios found in some of the studied sampling sites could also be related to the presence of additional Ni sources in the area, which impact can cause anomalously low V/Ni ratios even if these sites are also impacted by ship exhaust emissions (Moreno et al., 2010).

The contribution of this factor was quite homogeneous between sites, as observed in Figure 5. Only the contribution at the GUAR site was slightly higher; this could probably be related to the fact that the highest As concentrations were found at this site (see Table 4). In this regard, when a five-factor model was run, the main tracer of the additional factor was As and its contribution was focused on the GUAR site. Although the presence of a local As source in the vicinity of the GUAR site can not be rejected, the contribution of this source would be negligible with respect to the rest of the identified sources. Thus, a four-factor model was considered representative of the main metal(loid) emission sources in the area and this factor was considered a mixed factor, mainly attributed to oil combustion processes, more likely to ship exhaust emissions from the Santander Bay.

3.4 Error estimation of the PMF model

Tables 8 and 9 present the error estimation associated with the contribution of the identified factors and with the contribution of the metals used as key tracers of the

sources, respectively. As Table 8 shows, the factor attributed to the mixed source presents the highest uncertainty, in agreement with its low mass contribution. For non-exhaust traffic emissions results are quite stable, as indicated by DISP, BS and BS-DISP tests. On the contrary, while the point source emissions from the manganese alloy plant seem to be more sensitive to the BS and BS-DISP tests, fugitive emissions present a greater sensitivity only to the BS-DISP test. This could indicate the greater difficulty in fitting two factors highly affected by the changes in emission patterns of the plant and the different wind scenarios. On the other hand, Table 9 shows the uncertainty related to the contribution of the metals used as key tracers for the interpretation of the PMF analysis. Among the metals widely associated with the identified sources, Mn, Cd, Cu and V were selected for being mainly concentrated in the specific source (i.e. 95% of the measured Mn concentration in the fugitive emissions from the manganese alloy plant, 82% of Cu in non-exhaust traffic emissions, 84% of Cd in the point source emissions and 76% of V in the mixed origin source). As can be observed, the uncertainty associated with the contribution of these metals in the respective sources is reasonably low, with the exception of Mn, which seems to be more sensitive to BS-DISP test, probably due to the high variability of this metal and the presence of several peak values in the dataset.

4. Conclusions

In this study, the levels and emission sources of eleven metal(loid)s (i.e. V, Mn, Fe, Ni, Cu, Zn, As, Mo, Cd, Sb and Pb) have been investigated in seven sites located in an urban area characterized by the proximity of several metal(loid) sources (mainly a manganese alloy plant). The highest concentrations were found for Mn, Fe, Zn, Pb and Cu, with Mn being a metal of special concern. Although short sampling campaigns (i.e. 28 consecutive days) have been developed at each site, the results found in this study

suggest that air Mn concentrations would exceed by far the annual mean value established by the World Health Organization (WHO) as a guideline (i.e. 150 ng/m^3) in the studied area. The highest mean concentrations of most metal(loid)s were found at the sites located N-NW from the manganese alloy plant, in the direction of the prevailing winds of the region during the sampling period. Strong correlations were found between most metals frequently associated with the manganese alloy industry (i.e. Mn, Fe, Zn, Cd and Pb) and between those metal(loid)s linked to non-exhaust traffic emissions (i.e. Fe, Zn, Cu, Sb and Mo).

The multi-site dataset composed of the eleven metal(loid) concentrations was evaluated in a single run by positive matrix factorization (PMF). Four metal(loid) sources were identified: Fugitive and point source emissions from the manganese alloy plant (49.9% and 9.9%, respectively), non-exhaust traffic emissions (38.3%) and a source of mixed origin, mainly attributed to ship exhaust emissions (1.8%). The PMF analysis was able to make a clear separation between two different sources from the manganese alloy plant, which represented almost 60 % of the total measured metal(loid) levels, more than 80% of these emissions being assigned to fugitive emissions. These results will be useful for the assessment of the health risk associated with PM_{10}-bound metal(loid) exposure and for the design of efficient abatement strategies in areas impacted by similar industries.

Acknowledgements

This work was financially supported by the Spanish Ministry of Economy and Competitiveness (MINECO) through the CTM2013-43904R Project. Ana Hernández-Pellón would like to thank the Ministry of Economy and Competitiveness (MINECO) for the FPI and research stay grants awarded, reference numbers BES-2014-068790 and EEBB-I-17-12031.

References

Agarwal, A., Mangal, A., Satsangi, A., Lakhani, A., Maharaj Kumari, K., 2017. Characterization, sources and health risk analysis of $PM_{2.5}$ bound metals during foggy and non-foggy days in sub-urban atmosphere of Agra. Atmos. Res. 197, 121–131. doi:10.1016/j.atmosres.2017.06.027

Al-Harbi, M., 2014. Assessment of Air Quality in two Different Urban Localities. Int. J. Environ. Res. 8(1), 15–26.

Alleman, L.Y., Lamaison, L., Perdrix, E., Robache, A., Galloo, J.C., 2010. PM_{10} metal concentrations and source identification using positive matrix factorization and wind sectoring in a French industrial zone. Atmos. Res. 96, 612–625. doi:10.1016/j.atmosres.2010.02.008

Argyropoulos, G., Samara, C., Diapouli, E., Eleftheriadis, K., Papaoikonomou, K., Kungolos, A., 2017. Source apportionment of PM_{10} and $PM_{2.5}$ in major urban Greek agglomerations using a hybrid source-receptor modeling process. Sci. Total Environ. 601–602, 906–917. doi:10.1016/j.scitotenv.2017.05.088

Arruti, A., Fernández-Olmo, I., Irabien, A., 2011. Regional evaluation of particulate matter composition in an Atlantic coastal area (Cantabria region, northern Spain): Spatial variations in different urban and rural environments. Atmos. Res. 101, 280–293. doi:10.1016/j.atmosres.2011.03.001

Bari, A., Kindzierski, W.B., 2018. Ambient volatile organic compounds (VOCs) in communities of the Athabasca oil sands region: Sources and screening health risk. Environ. Pollut. 235, 602–614. doi:10.1016/j.envpol.2017.12.065

Belis, C.A., Karagulian, F., Amato, F., Almeida, M., Artaxo, P., Beddows, D.C.S., Bernardoni, V., Bove, M.C., Carbone, S., Cesari, D., Contini, D., Cuccia, E., Diapouli, E., Eleftheriadis, K., Favez, O., El Haddad, I., Harrison, R.M., Hellebust, S., Hovorka, J., Jang, E., Jorquera, H., Kammermeier, T., Karl, M., Lucarelli, F., Mooibroek, D., Nava, S., Nøjgaard, J.K., Paatero, P., Pandolfi, M., Perrone, M.G., Petit, J.E., Pietrodangelo, A., Pokorná, P., Prati, P., Prevot, A.S.H., Quass, U., Querol, X., Saraga, D., Sciare, J., Sfetsos, A., Valli, G., Vecchi, R., Vestenius, M., Yubero, E. Hopke, P.K., 2015. A new methodology to assess the performance and uncertainty of source

apportionment models II: The results of two European intercomparison exercises. Atmos. Environ. 123, 240-250. doi:10.1016/j.atmosenv.2015.10.068

Belis, C.A., Karagulian, F., Larsen, B.R., Hopke, P.K., 2013. Critical review and meta-analysis of ambient particulate matter source apportionment using receptor models in Europe. Atmos. Environ. 69, 94–108. doi:10.1016/j.atmosenv.2012.11.009

Bjørklund, G., Chartrand, M.S., Aaseth, J., 2017. Manganese exposure and neurotoxic effects in children. Environ. Res. 155, 380–384. doi:10.1016/j.envres.2017.03.003

Bove, M.C., Massabò, D., Prati, P., 2018. PMF5.0 vs. CMB8.2: An inter-comparison study based on the new European SPECIEUROPE database. Atmos. Res. 201, 181–188. doi:10.1016/j.atmosres.2017.10.021

Brown, S.G., Eberly, S., Paatero, P., Norris, G.A., 2015. Methods for estimating uncertainty in PMF solutions: Examples with ambient air and water quality data and guidance on reporting PMF results. Sci. Total Environ. 518–519, 626–635. doi:10.1016/j.scitotenv.2015.01.022

Carslaw, D.C., 2015. The openair manual-open-source tools for analyzing air pollution data. Manual for version 1.1-4, King's College London.

Carslaw, D.C., Ropkins, K., 2012. Openair - an R package for air quality data analysis. Environ. Modell. Softw. 27–28, 52–61. doi:10.1016/j.envsoft.2011.09.008

Carter, M.R., Gaudet, B.J., Stauffer, D.R., White, T.S., Brantley, S.L., 2015. Using soil records with atmospheric dispersion modeling to investigate the effects of clean air regulations on 60 years of manganese deposition in Marietta, Ohio (USA). Sci. Total Environ. 515–516, 49–59. doi:10.1016/j.scitotenv.2015.01.015

Cesari, D., Contini, D., Genga, A., Siciliano, M., Elefante, C., Baglivi, F., Daniele, L., 2012. Analysis of raw soils and their re-suspended PM_{10} fractions: Characterisation of source profiles and enrichment factors. Appl. Geochemistry 27(6), 1238–1246. doi:10.1016/j.apgeochem.2012.02.029

Cesari, D., Donateo, A., Conte, M., Contini, D., 2016. Inter-comparison of source apportionment of PM10 using PMF and CMB in three sites nearby an industrial area in central Italy. Atmos. Res., 182, 282-293. doi:10.1016/j.atmosres.2016.08.003

Chen, P., Culbreth, M., Aschner, M., 2016. Exposure, epidemiology, and mechanism of the environmental toxicant manganese. Environ. Sci. Pollut. Res. 23, 13802–13810. doi:10.1007/s11356-016-6687-0

Contini, D., Cesari, D., Conte, M., Donateo, A., 2016. Application of PMF and CMB receptor models for the evaluation of the contribution of a large coal-fired power plant to PM10 concentrations. Sci. Total Environ, 560-561, 131-140. doi:10.1016/j.scitotenv.2016.04.031

Contini, D., Belosi, F., Gambaro, A., Cesari, D., Stortini, A. M., Bove, M. C., 2012. Comparison of PM10 concentrations and metal content in three different sites of the Venice Lagoon: An analysis of possible aerosol sources. J. Environ. Sci. (China), 24(11), 1954-1965. doi:10.1016/S1001-0742(11)61027-9

Deng, J., Zhang, Y., Qiu, Y., Zhang, H., Du, W., Xu, L., Hong, Y., Chen, Y., Chen, J., 2018. Source apportionment of $PM_{2.5}$ at the Lin'an regional background site in China with three receptor models. Atmos. Res. 202, 23–32. doi:10.1016/j.atmosres.2017.11.017

Di Gilio, A., Ventrella, G., Giungato, P., Tutino, M., Giua, R., Assennato, G., de Gennaro, G., 2017. An intensive monitoring campaign of PAHs for assessing the impact of a steel plant. Chemosphere, 168, 171-182. doi:10.1016/j.chemosphere.2016.10.019

Dongarrà, G., Manno, E., Varrica, D., 2009. Possible markers of traffic-related emissions. Environ. Monit. Assess. 154(1-4), 117–125. doi:10.1007/s10661-008-0382-7

European Commission. Joint Research Centre. Institute of Energy and Transport, 2014. Non-exhaust traffic related emissions. Brake and tyre wear PM. JCR Science and Policy Reports. Luxembourg. ISSN 1831-9424.

European Commission. Joint Research Centre. Institute for Environment and Sustainability, 2013. European Guide on Air Pollution Source Apportionment with Receptor Models. JRC Reference Reports. Luxembourg. ISBN 978-92-79-32513-7.

Fiordelisi, A., Piscitelli, P., Trimarco, B., Coscioni, E., Iaccarino, G., Sorriento, D., 2017. The mechanisms of air pollution and particulate matter in cardiovascular diseases. Heart Fail. Rev. 22, 337–347. doi:10.1007/s10741-017-9606-7

Fomba, K.W., van Pinxteren, D., Müller, K., Spindler, G., Herrmann, H., 2017. Assessment of trace metal levels in size-resolved particulate matter in the area of Leipzig. Atmos. Environ. 176, 60–70. doi:10.1016/j.atmosenv.2017.12.024

Fragkou, E., Douros, I., Moussiopoulos, N., Belis, C.A., 2012. Current trends in the use of models for source apportionment of air pollutants in Europe. Int. J. Environ. Pollut. 50, 363–375. doi:10.1504/IJEP.2012.051207

Friend, A.J., Ayoko, G.A., Jager, D., Wust, M., Jayaratne, E.R., Jamriska, M., Morawska, L., 2013. Sources of ultrafine particles and chemical species along a traffic corridor: Comparison of the results from two receptor models. Environ. Chem. 10, 54–63. doi:10.1071/EN12149

Fulk, F., Haynes, E.N., Hilbert, T.J., Brown, D., Petersen, D., Reponen, T., 2016. Comparison of stationary and personal air sampling with an air dispersion model for children's ambient exposure to manganese. J. Expo. Sci. Environ. Epidemiol. 26, 494–502. doi:10.1038/jes.2016.30

Gjønnes, K., Skogstad, A., Hetland, S., Ellingsen, D. G., Thomassen, Y., Weinbruch, S. 2011. Characterisation of workplace aerosols in the manganese alloy production industry by electron microscopy. Anal. Bioanal. Chem. 399(3), 1011–1020. doi:10.1007/s00216-010-4470-5

Grange, S.K., Lewis, A.C., Carslaw, D.C., 2016. Source apportionment advances using polar plots of bivariate correlation and regression statistics. Atmos. Environ. 145, 128–134. doi:10.1016/j.atmosenv.2016.09.016

Gregoris, E., Barbaro, E., Morabito, E., Toscano, G., Donateo, A., Cesari, D., Contini, D., Gambaro, A., 2016. Impact of maritime traffic on polycyclic aromatic hydrocarbons, metals and particulate matter in Venice air. Environ. Sci. Pollut. Res., 23(7), 6951-6959. doi:10.1007/s11356-015-5811-x

Gunst, S., Weinbruch, S., Wentzel, M., Ortner, H. M., Skogstad, A., Hetland, S., Thomassen, Y., 2000. Chemical composition of individual aerosol particles in

workplace air during production of manganese alloys. J. Environ. Monit. 2(1), 65–71. doi:10.1039/a908329d

Hernández-Pellón A., Fernández-Olmo I., 2016. Monitoring the levels of particle matter-bound manganese: An intensive campaign in an urban/industrial area. Conference Proceedings 2nd International Conference on Atmospheric Dust - DUST2016. ProScience 3, 50-55.

Hopke, P.K., 2016. Review of receptor modeling methods for source apportionment. J. Air Waste Manage. Assoc. 66, 237–259. doi:10.1080/10962247.2016.1140693

Hopke, P.K., Cohen, D.D., 2011. Application of receptor modeling methods. Atmos. Pollut. Res. 2, 122–125. doi:10.5094/APR.2011.016

International Agency for Research on Cancer (IARC), 2016. IARC Monographs on the Evaluation of Carcinogenic Risks to Humans. Outdoor air pollution. Volume 109.

Kara, M., Hopke, P.K., Dumanoglu, Y., Altiok, H., Elbir, T., Odabasi, M., Bayram, A., 2015. Characterization of PM using multiple site data in a heavily industrialized region of Turkey. Aerosol Air Qual. Res. 15, 11–27. doi:10.4209/aaqr.2014.02.0039

Kelly, F.J., Fussell, J.C., 2012. Size, source and chemical composition as determinants of toxicity attributable to ambient particulate matter. Atmos. Environ. 60, 504–526. doi:10.1016/j.atmosenv.2012.06.039

Kero, I., Naess, M.K., Tranell, G., 2015. Particle size distributions of particulate emissions from the ferroalloy industry evaluated by electrical low pressure impactor (ELPI). J. Occup. Environ. Hyg. 12(1), 37-44. doi:10.1080/15459624.2014.935783

Leoni, C., Pokorná, P., Hovorka, J., Masiol, M., Topinka, J., Zhao, Y., Křůmal, K., Cliff, S., Mikuška, P., Hopke, P.K., 2018. Source apportionment of aerosol particles at a European air pollution hot spot using particle number size distributions and chemical composition. Environ. Pollut. 234, 145–154. doi:10.1016/j.envpol.2017.10.097

Lipfert, F.W., 2018. Long-term associations of morbidity with air pollution: A catalog and synthesis. J. Air Waste Manag. Assoc. 68(1), 12–28. doi:10.1080/10962247.2017.1349010

Manousakas, M., Papaefthymiou, H., Diapouli, E., Migliori, A., Karydas, A.G., Bogdanovic-Radovic, I., Eleftheriadis, K., 2017. Assessment of $PM_{2.5}$ sources and their corresponding level of uncertainty in a coastal urban area using EPA PMF 5.0 enhanced diagnostics. Sci. Total Environ. 574, 155–164. doi:10.1016/j.scitotenv.2016.09.047

Marris, H., Deboudt, K., Augustin, P., Flament, P., Blond, F., Fiani, E., Fourmentin, M., Delbarre, H., 2012. Fast changes in chemical composition and size distribution of fine particles during the near- field transport of industrial plumes. Sci. Total Environ. 427–428, 126–138. doi:10.1016/j.scitotenv.2012.03.068

Mbengue, S., Alleman, L., Flament, P., 2015. Bioaccessibility of trace elements in fine and ultrafine atmospheric particles in an industrial environment. Environ. Geochem. Health. 37(5), 875-889. doi:10.1007/s10653-015-9756-2

Moldanová, J., Fridell, E., Winnes, H., Holmin-Fridell, S., Boman, J., Jedynska, A., Tishkova, V., Demirdjian, B., Joulie, S., Bladt, H., Ivleva, N.P., Niessner, R., 2013. Physical and chemical characterisation of PM emissions from two ships operating in European emission control areas. Atmos. Meas. Tech. 6(12), 3577-3596. doi:10.5194/amtd-6-3931-2013

Moreno, T., Pandolfi, M., Querol, X., Lavín, J., Alastuey, A., Viana, M., Gibbons, W., 2011. Manganese in the urban atmosphere: Identifying anomalous concentrations and sources. Environ. Sci. Pollut. Res. 18, 173–183. doi:10.1007/s11356-010-0353-8

Moreno, T., Querol, X., Alastuey, A., de la Rosa, J., Sánchez de la Campa, A.M., Minguillón, M., Pandolfi, M., González-Castanedo, Y., Monfort, E., Gibbons, W., 2010. Variations in vanadium, nickel and lanthanoid element concentrations in urban air. Sci. Total Environ. 408(20), 4569–4579. doi:10.1016/j.scitotenv.2010.06.016

Mukherjee, A., Agrawal, M., 2018. Air pollutant levels are 12 times higher than guidelines in Varanasi, India. Sources and transfer. Environ. Chem. Lett. 1-8. doi:10.1007/s10311-018-0706-y

Mukherjee, A., Agrawal, M., 2017. World air particulate matter: sources, distribution and health effects. Environ. Chem. Lett. 15(2), 283–309. doi:10.1007/s10311-017-0611-9

Ogundele, L.T., Owoade, O.K., Olise, F.S., Hopke, P.K., 2016. Source identification and apportionment of $PM_{2.5}$ and $PM_{2.5–10}$ in iron and steel scrap smelting factory environment using PMF, PCFA and UNMIX receptor models. Environ. Monit. Assess. 188(10). doi:10.1007/s10661-016-5585-8

Orogade, S.A., Owoade, K.O., Hopke, P.K., Adie, D.B., Ismail, A., Okuofu, C.A., 2016. Source apportionment of fine and coarse particulate matter in industrial areas of Kaduna Northern Nigeria. Aerosol Air Qual. Res. 16, 1179–1190. doi:10.4209/aaqr.2015.11.0636

Otero-Pregigueiro, D., Hernández-Pellón, A., Borge, R., Fernández-Olmo, I., 2018. Estimation of PM_{10}-bound manganese concentration near a ferromanganese alloy plant by atmospheric dispersion modelling. Sci. Total Environ. 627, 534–543. doi:10.1016/j.scitotenv.2018.01.246

Owoade, K.O., Hopke, P.K., Olise, F.S., Ogundele, L.T., Fawole, O.G., Olaniyi, B.H., Jegede, O.O., Ayoola, M.A., Bashiru, M.I., 2015. Chemical compositions and source identification of particulate matter ($PM_{2.5}$ and $PM_{2.5–10}$) from a scrap iron and steel smelting industry along the Ife–Ibadan highway, Nigeria. Atmos. Pollut. Res. 6, 107–119. doi:10.5094/APR.2015.013

Paatero, P., Eberly, S., Brown, S.G., Norris, G.A., 2014. Methods for estimating uncertainty in factor analytic solutions. Atmos. Meas. Tech. 7, 781–797. doi:10.5194/amt-7-781-2014

Pandolfi, M., Gonzalez-Castanedo, Y., Alastuey, A., de la Rosa, J.D., Mantilla, E., de la Campa, A.S., Querol, X., Pey, J., Amato, F. Moreno, T., 2011. Source apportionment of PM_{10} and $PM_{2.5}$ at multiple sites in the strait of Gibraltar by PMF: Impact of shipping emissions. Environ. Sci. Pollut. Res., 18 (2), 260-269. doi:10.1007/s11356-010-0373-4

Pernigotti, D., Belis, C.A., Spanò, L., 2016. SPECIEUROPE : The European data base for PM source profiles. Atmos. Pollut. Res. 7(2), 307-314.doi:10.1016/j.apr.2015.10.007

Popovicheva, O., Kireeva, E., Shonija, N., Zubareva, N., Persiantseva, N., Tishkova, V., Demirdjian, B., Moldanová, J. Mogilnikov, V., 2009. Ship particulate pollutants: Characterization in terms of environmental implication. J. Environ. Monit. 11(11), 2077-2086. doi:10.1039/b908180a

Querol, X., Viana, M., Alastuey, A., Amato, F., Moreno, T., Castillo, S., Pey, J., de la Rosa, J., Sánchez de la Campa, A., Artíñano, B., Salvador, P., García Dos Santos, S., Fernández-Patier, R., Moreno-Grau, S., Negral, L., Minguillón, M.C., Monfort, E., Gil, J.I., Inza, A., Ortega, L.A., Santamaría, J.M., Zabalza, J., 2007. Source origin of trace elements in PM from regional background, urban and industrial sites of Spain. Atmos. Environ. 41, 7219–7231. doi:10.1016/j.atmosenv.2007.05.022

Ramírez, O., Sánchez de la Campa, A.M., Amato, F., Catacolí, R.A., Rojas, N.Y., de la Rosa, J., 2018. Chemical composition and source apportionment of PM_{10} at an urban background site in a high–altitude Latin American megacity (Bogota, Colombia). Environ. Pollut. 233, 142–155. doi:10.1016/j.envpol.2017.10.045

Reff, A., Eberly, S.I., Bhave, P. V., 2007. Receptor modeling of ambient particulate matter data using positive matrix factorization: Review of existing methods. J. Air Waste Manage. Assoc. 57, 146–154. doi:10.1080/10473289.2007.10465319

Ruiz, S., Fernández-Olmo, I., Irabien, A., 2014. Discussion on graphical methods to identify point sources from wind and particulate matter-bound metal data. Urban Clim. 10, 671–681. doi:10.1016/j.uclim.2013.11.001

Sjödin, A., Ferm, M., Björk, A., Rahmberg, M., Gudmundsson, A., Swietlicki, E., Johansson, C., Gustafsson, M., Blomquist, G., 2010. Wear particles from road traffic - A field, laboratory and modelling study. Final Report. IVL, Swedish Environmental Research Institute.

Sofowote, U.M., Su, Y., Dabek-Zlotorzynska, E., Rastogi, A.K., Brook, J., Hopke, P.K., 2015a. Sources and temporal variations of constrained PMF factors obtained from multiple-year receptor modeling of ambient $PM_{2.5}$ data from five speciation sites in Ontario, Canada. Atmos. Environ. 108, 140–150. doi:10.1016/j.atmosenv.2015.02.055

Sofowote, U.M., Su, Y., Dabek-zlotorzynska, E., Rastogi, A.K., Brook, J., Hopke, P.K., 2015b. Constraining the factor analytical solutions obtained from multiple-year receptor

modeling of ambient $PM_{2.5}$ data from five speciation sites in Ontario, Canada. Atmos. Environ. 108, 151–157. doi:10.1016/j.atmosenv.2015.02.045

Spada, N., Bozlaker, A., Chellam, S., 2012. Multi-elemental characterization of tunnel and road dusts in Houston, Texas using dynamic reaction cell-quadrupole-inductively coupled plasma-mass spectrometry: Evidence for the release of platinum group and anthropogenic metals from motor vehicles. Anal. Chim. Acta 735, 1–8. doi:10.1016/j.aca.2012.05.026

Squizzato, S., Cazzaro, M., Innocente, E., Visin, F., Hopke, P.K., Rampazzo, G., 2017. Urban air quality in a mid-size city - $PM_{2.5}$ composition, sources and identification of impact areas: From local to long range contributions. Atmos. Res. 186, 51–62. doi:10.1016/j.atmosres.2016.11.011

Streibel, T., Schnelle-Kreis, J., Czech, H., Harndorf, H., Jakobi, G., Jokiniemi, J., Karg, E., Lintelmann, J., Matuschek, G., Michalke, B., Müller, L., Orasche, J., Passig, J., Radischat, C., Rabe, R., Reda, A., Rüger, C., Schwemer, T., Sippula, O., Stengel, B., Sklorz, M., Torvela, T., Weggler, B., Zimmermann, R., 2017. Aerosol emissions of a ship diesel engine operated with diesel fuel or heavy fuel oil. Environ. Sci. Pollut. Res. 24(12), 10976–10991. doi:10.1007/s11356-016-6724-z

Uria-Tellaetxe, I., Carslaw, D.C., 2014. Conditional bivariate probability function for source identification. Environ. Model. Softw. 59, 1–9. doi:10.1016/j.envsoft.2014.05.002

U.S. Environmental Protection Agency (EPA). Office of Research and Development, 2016. SPECIATE Version 4.5. Database Development Documentation. Final Report. EPA/600/R-16/294.

U.S. Environmental Protection Agency (EPA). Office of Research and Development, 2014. EPA Positive Matrix Factorization (PMF) 5.0. Fundamentals and User Guide. Washington. EPA/600/R-14/108.

Viana, M., Amato, F., Alastuey, A., Moreno, T., Dos Santos, S.G., Herce, M.D., Fernández-Patier, R., 2009. Chemical tracers of particulate emissions from commercial shipping. Environ. Sci. Technol. 43(19), 7472–7477.

Viana, M., Kuhlbusch, T.A.J., Querol, X., Alastuey, A., Harrison, R.M., Hopke, P.K., Winiwarter, W., Vallius, M., Szidat, S., Prévôt, A.S.H., Hueglin, C., Bloemen, H., Wåhlin, P., Vecchi, R., Miranda, A.I., Kasper-Giebl, A., Maenhaut, W., Hitzenberger, R., 2008a. Source apportionment of particulate matter in Europe: A review of methods and results. J. Aerosol. Sci. 39(10), 827–849. doi:10.1016/j.jaerosci.2008.05.007

Viana, M., Pandolfi, M., Minguillón, M.C., Querol, X., Alastuey, A., Monfort, E., Celades, I., 2008b. Inter-comparison of receptor models for PM source apportionment: Case study in an industrial area. Atmos. Environ. 42(16), 3820–3832. doi:10.1016/j.atmosenv.2007.12.056

Viana, M., Querol, X., Götschi, T., Alastuey, A., Sunyer, J., Forsberg, B., Heinrich, J., Norbäck, D., Payo, F., Maldonado, J.A., Künzli, N., 2007. Source apportionment of ambient $PM_{2.5}$ at five Spanish centres of the European community respiratory health survey (ECRHS II). Atmos. Environ. 41(7), 1395–1406. doi:10.1016/j.atmosenv.2006.10.016

Wang, Y., Xiong, L., Tang, M., 2017. Toxicity of inhaled particulate matter on the central nervous system: neuroinflammation, neuropsychological effects and neurodegenerative disease. J. Appl. Toxicol. 37, 644–667. doi:10.1002/jat.3451

Watson, J.G., Chen, L.-W.A., Chow, J.C., Doraiswamy, P., Lowenthal, D.H., 2012. Source apportionment: Findings from the U.S. supersites program. J. Air Waste Manage. Assoc. 58(2), 265-288. doi:10.3155/1047-3289.58.2.265

WHO, 2016a. Ambient (outdoor) air quality and health. Fact sheet. Available at: http://www.who.int/mediacentre/factsheets/fs313/en/

WHO. Regional Office for Europe, 2016b. Health risk assessment of air pollution-general principles. Copenhagen. ISBN 978 92 890 51316.

Wu, D., Zhang, F., Lou, W., Li, D., Chen, J., 2017. Chemical characterization and toxicity assessment of fine particulate matters emitted from the combustion of petrol and diesel fuels. Sci. Total Environ. 605-606, 172–179. doi:10.1016/j.scitotenv.2017.06.058

Zhang, J., Zhou, X., Wang, Z., Yang, L., Wang, J., Wang, W., 2018. Trace elements in $PM_{2.5}$ in Shandong Province: Source identification and health risk assessment. Sci. Total Environ. 621, 558–577. doi:10.1016/j.scitotenv.2017.11.292

Table 1. Sampling sites of the PM_{10} sampling campaign: Name, code, location and distance from the manganese alloy plant.

Site code	Site description	Coordinates (UTM)	Distance (m)
CROS	Official monitoring site (CIMA)	X= 431916, Y= 4807982	850
GUAR	Official monitoring site (CIMA)	X= 432146, Y= 4806368	790
CULTJH	Juan de Herrera Cultural Center	X= 432707, Y= 4807473	800
CPJH	Juan de Herrera Public School	X= 432205, Y= 4807473	400
CCV	La Vidriera Cultural Center	X= 431899, Y= 4807290	350
CMFC	Cros Municipal Center for training	X= 432128, Y= 4808086	1130
GUARCRC	Garden of a private house (Guarnizo)	X= 430673, Y= 4804933	2450

Table 2. Metal recovery (%) obtained for SRM 1648a and detection limits (ng/m^3) calculated for the determination of the total metal(loid) content.

Element	Recovery (%)	Detection limit (ng/m3)
	SRM 1648a	Quartz fiber filters
V	82±3	0.03
Mn	90±4	2.2
Fe	87±4	43.7
Ni	91±7	2.1
Cu	90±4	0.48
Zn	82±7	51.6
As	86±7	0.01
Mo	n.a.	0.4
Cd	91±4	0.01
Sb	72±8	0.08
Pb	92±6	0.26

n.a.: certificated value not available for the reference material (SRM 1648a)

Table 3. Summary of PMF settings.

Parameter	PMF analysis in this study
Data type; Time frame	PM_{10}; 24h
N sites	7
N species	11+total variable
Weak species	Ni, Mo
N samples	196
Treatment of data below detection limit (DL)	0.5*DL
Error fraction (EF)	0.1
Treatment of outliers[a]	>1.5*P95=P50
N factors	2-5
N runs	100
% Extra modeling uncertainty	0%
Robust mode	Yes
Constraints	None
Seed value	Random
N bootstraps in BS; r^2 for BS	100; 0.8
BS block size	6
DISP dQmax	4, 8 15, 25
DISP active species	All except Ni and Mo
N bootstraps; r^2 for BS in BS-DISP	100; 0.8
BS-DISP active species	Mn, Cu, Cd, V
BS-DISP dQmax	0.5, 1, 2, 4
Fpeak	From -5 to 5

[a] Values above 1.5 times the 95th percentile were replaced by the 50th percentile

Table 4. Total metal(loid) content (ng/m^3) in PM_{10} at the studied locations

Element	CROS[a]		GUAR[b]		CULTJH[c]		CPJH[d]		CCV[e]		CMFC[f]		GUARCRC[g]	
	Mean*	SD	Mean*	SD	Mean*	SD	Mean*	SD	Mean*	SD	Mean*	SD	Mean*	SD
V	0.55	0.36	1.54	1.25	1.64	0.53	1.46	0.65	1.69	0.95	1.15	0.69	1.05	0.66
Mn	266.7	450.6	156.2	226.6	208.0	319.1	713.9	653.8	721.9	654.1	589.2	575.2	25.4	29.9
Fe	280.9	268.6	275.7	195.5	223.7	207.5	246.3	127.2	322.0	192.8	645.0	360.0	482.7	362.5
Ni	1.40	1.19	2.58	2.57	1.68	2.18	2.24	1.52	1.39	0.77	2.52	5.69	1.49	1.02
Cu	10.10	10.03	8.91	7.90	3.97	2.00	7.27	7.44	8.83	3.83	14.12	6.93	12.40	10.63
Zn	101.5	119.5	159.9	69.0	74.9	64.4	136.1	131.6	198.6	145.0	172.9	163.8	153.2	82.3
As	0.16	0.19	1.89	4.30	0.16	0.08	0.31	0.13	0.38	0.18	0.20	0.15	0.40	0.41
Mo	0.42	0.40	0.48	0.38	0.31	0.28	0.27	0.13	0.83	2.05	0.47	0.67	0.61	0.48
Cd	0.54	0.74	0.57	0.70	0.61	0.50	3.11	3.86	3.47	3.51	2.23	2.89	0.39	0.45
Sb	0.64	0.62	0.71	0.50	0.34	0.19	0.40	0.24	0.68	0.37	1.14	0.99	0.76	1.06
Pb	18.5	25.0	16.2	13.3	17.6	16.1	47.0	57.8	44.8	38.6	38.6	31.9	7.8	7.4

a: 30 January-27 February. 28 daily samples; b: 4 March-1 April. 28 daily samples; c: 22 May-19 June. 28 daily samples; d: 23 July-21 August. 28 daily samples; e: 2 September-30 September 28 daily samples; f: 2 October-30 October. 28 daily samples; g: 14 November-13 December. 28 daily samples. Year: 2015.

*Arithmetic mean

Table 5. Spearman correlation coefficients between metal(loid)s associated with emissions from the manganese alloy industry.

Elements	CROS	GUAR	CULTJH	CPJH	CCV	CMFC	GUARCRC
Mn-Fe	**0.85**	0.47*	0.09	0.23	**0.74**	0.24	0.25*
Mn-Zn	**0.55**	**0.64**	-0.20	0.43*	**0.81**	**0.67**	**0.46**
Mn-Cd	**0.87**	**0.70**	-0.44	0.54	**0.84**	**0.83**	**0.75**
Mn-Pb	**0.84**	**0.85**	-0.30	0.37*	**0.83**	**0.76**	**0.68**
Fe-Zn	**0.65**	**0.64**	0.21	-0.04	**0.64**	0.34	0.43*
Fe-Cd	**0.75**	**0.70**	-0.04	0.02	**0.67**	0.21	**0.34**
Fe-Pb	**0.78**	**0.59**	0.14	0.11	**0.59**	0.09	**0.55**
Zn-Cd	**0.65**	**0.61**	0.36	**0.62**	**0.86**	**0.77**	**0.54**
Zn-Pb	**0.56**	**0.67**	0.30	**0.63**	**0.81**	**0.68**	**0.60**
Cd-Pb	**0.82**	**0.83**	**0.60**	**0.77**	**0.70**	**0.72**	**0.82**

In bold character correlation is significant at the 0.01 level.
*Correlation is significant at the 0.05 level.

Table 6. Spearman correlation coefficients between metal(loid)s associated with non-exhaust traffic emissions.

Elements	CROS	GUAR	CULTJH	CPJH	CCV	CMFC	GUARCRC
Fe-Cu	**0.84**	**0.83**	0.16	**0.70**	**0.84**	**0.57**	**0.58**
Fe-Sb	**0.83**	**0.81**	0.25	**0.64**	**0.69**	**0.48**	**0.67**
Fe-Mo	**0.53**	**0.75**	-0.01	0.46*	**0.63**	-0.18	**0.59**
Zn-Fe	**0.65**	**0.51**	0.21	-0.04	**0.64**	0.34	0.43*
Zn-Cu	**0.51**	**0.66**	0.38*	0.18	**0.52**	0.32	**0.48**
Zn-Sb	**0.56**	**0.68**	0.46*	0.24	0.41*	0.27	**0.49**
Zn-Mo	**0.58**	**0.58**	0.21	0.14	0.31	-0.06	**0.28**
Cu-Sb	**0.78**	**0.94**	**0.80**	**0.86**	**0.79**	**0.73**	**0.80**
Cu-Mo	**0.64**	**0.85**	-0.09	**0.61**	**0.64**	0.32	**0.75**
Sb-Mo	**0.54**	**0.84**	0.39*	0.41*	0.40*	0.40*	**0.89**

In bold character correlation is significant at the 0.01 level.
*Correlation significant at the 0.05 level.

Table 7. Summary of the PMF and error estimation diagnostics

Parameter	4 factors
$Q_{theoretical}$[a]	1328
Q_{robust}[b]	7723.5
Q_{true}[c]	9846.6
$Q_{robust}/Q_{theoretical}$	5.8
Fpeak	0
DISP % dQ	<0.1%
DISP swaps	0
Factors with BS Mapping <100%	Fugitive sources from Mn alloy plant (91%)
BS-DISP % cases with swaps	2%

[a] $Q_{theoretical}$=nm-p(n+m); n: number of species, m: number of samples, p: number of factors.
[b] Q_{robust}: Goodness-of-fit parameter calculated excluding points not fit by the model
[c] Q_{true}: Goodness-of-fit parameter calculated including all points

Table 8. Error estimation summary: Factor contribution in µg/m^3

Factor	Base value	DISP min	DISP max	BS 5th	BS 95th	BS-DISP 5th	BS-DISP 95th
FE-MP	0.4	0.3	0.5	0.3	0.4	0.05	0.4
PS-MP	0.08	0.05	0.1	0.06	0.4	0.04	0.4
T	0.3	0.2	0.4	0.2	0.3	0.2	0.4
MS	0.02	0.01	0.2	0.01	0.1	0.0	0.2

FE-MP: Fugitive emissions from the manganese alloy plant
PS-MP: Point sources from the manganese alloy plant
T: Non-exhaust traffic emissions
MS: Mixed source

Table 9. Error estimation summary: Contribution of metals used as tracers for the specific factors in µg/m^3

Metal	Source	Base value	DISP min	DISP max	BS 5th	BS 95th	BS-DISP 5th	BS-DISP 95th
Mn	FE-MP	0.351	0.301	0.376	0.291	0.350	0.000	0.376
Cu	T	0.007	0.005	0.008	0.005	0.007	0.005	0.008
Cd	PS-MP	0.0009	0.0008	0.001	0.0005	0.001	0.0006	0.001
V	MS	0.0008	0.0008	0.001	0.0002	0.001	0.0006	0.001

FE-MP: Fugitive emissions from the manganese alloy plant
PS-MP: Point sources from the manganese alloy plant
T: Non-exhaust traffic emissions
MS: Mixed source

Figure captions

Figure 1. Location of the sampling points and manganese alloy plant.

Figure 2. Wind roses calculated at the studied area during the sampling period (2015): (a) CROS site (30 January-27 February); (b) GUAR site (4 March-1 April); (c) CULTJH site (22 May-19 June), (d) CPJH site (23 July-21 August); (e) CCV site (2 September-30 September), (f) CMFC site (2 October-30 October); (g) GUARCRC site (14 November-13 December). Wind roses developed with Openair tools. According to Beaufort scale, calm criteria: 0.28 m/s.

Figure 3. Time series of Mn, Zn, Cd and Pb concentrations in PM_{10} samples collected at the CROS (a) and CCV (b) sites. Time series of Fe, Cu, Sb and Mo concentrations in PM_{10} samples collected at the CROS (c) and GUAR (d) and GUARCRC (e) sites.

Figure 4. Source profiles of the four factors obtained by PMF at the studied sites.

Figure 5. Time series of the factor contributions obtained by PMF at the studied sites.

Figure 6. Comparison between the factor profiles from PMF and the calculated factor profiles from identified factors: (a) Point source emissions from the manganese alloy plant located in the area of study, reported in the e-PRTR 2015; (b) Baghouse samples from a manganese alloy plant (0-10 μm). Source: EPA Speciate 4.5 (profile 2840110); (c) Raw materials mixing from a manganese alloy plant (Gunst et al., 2000); (d) Resuspended PM_{10} road dust from an urban-traffic area in Italy, reported by Cesari et al. (2012). Source: Specieurope database v2.0.

Figure 7. Comparison of the CBPF plots for the 75^{th} percentile of the contributions of the factor profiles associated with the fugitive and point-source emissions from the manganese alloy plant at the nearest receptor sites where samples were collected during the cold period: CROS (a), GUAR (b). Ws: Wind speed (m/s)

Figure 8. Comparison of the CBPF plots for the 75^{th} percentile of the contributions of the factor profiles associated with the fugitive and point-source emissions from the manganese alloy plant at the nearest receptor sites where samples were collected during the warm period: CCV (a), CPJH (b). Ws: Wind speed (m/s)

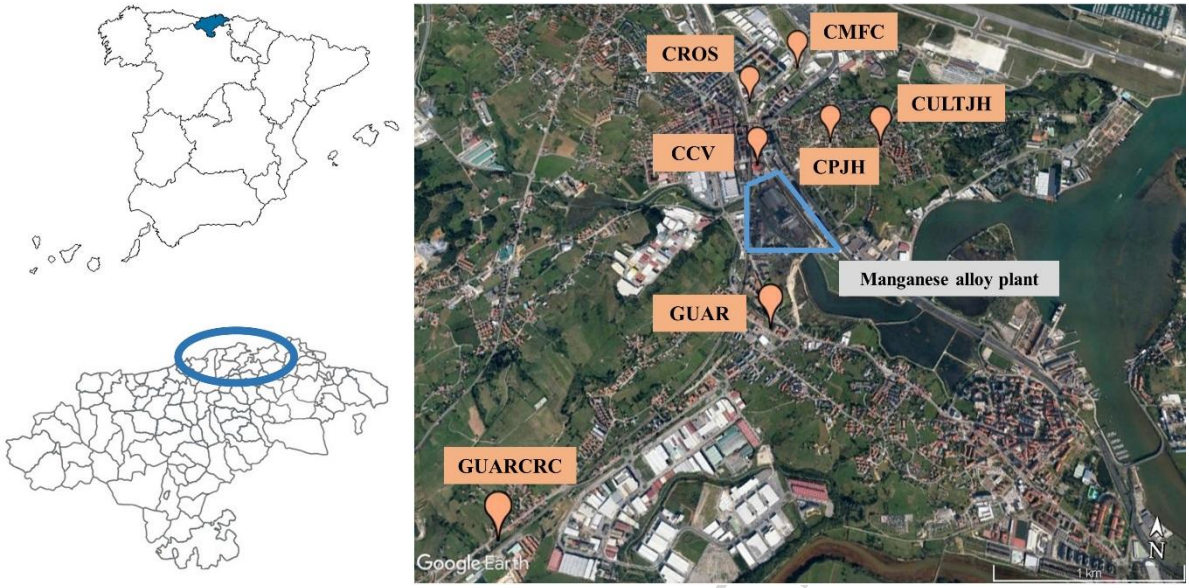

Figure 1. Location of the sampling points and manganese alloy plant.

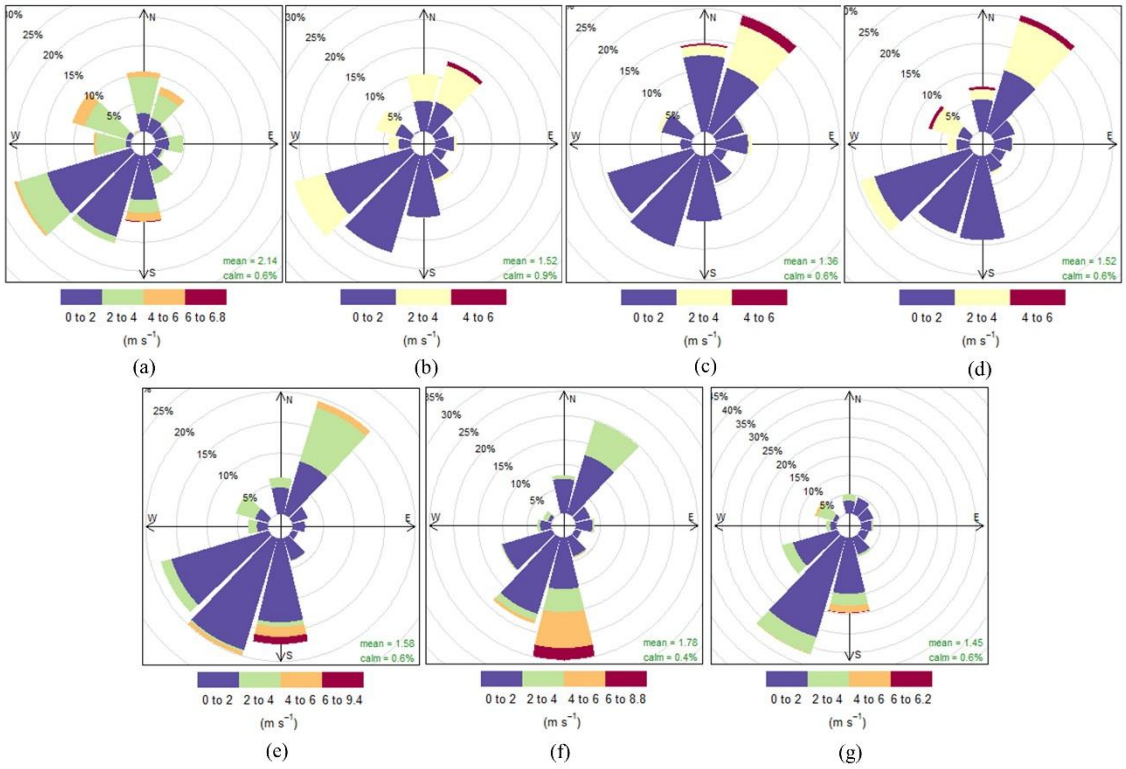

Figure 2. Wind roses calculated at the studied area during the sampling period (2015): (a) CROS site (30 January-27 February); (b) GUAR site (4 March-1 April); (c) CULTJH site (22 May-19 June), (d) CPJH site (23 July-21 August); (e) CCV site (2 September-30 September), (f) CMFC site (2 October-30 October); (g) GUARCRC site (14 November-13 December). Wind roses developed with Openair tools. According to Beaufort scale, calm criteria: 0.28 m/s.

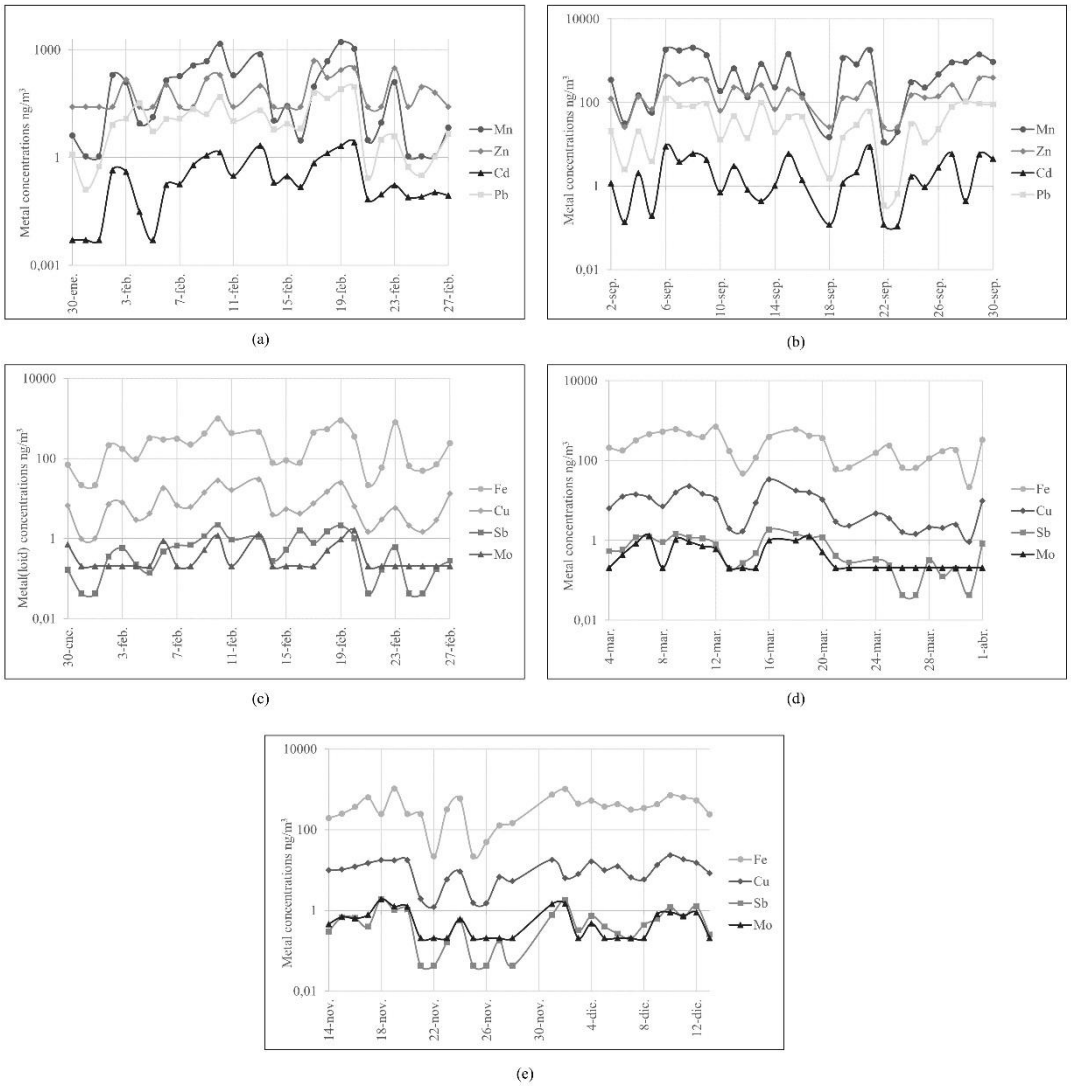

Figure 3. Time series of Mn, Zn, Cd and Pb concentrations in PM_{10} samples collected at the CROS (a) and CCV (b) sites. Time series of Fe, Cu, Sb and Mo concentrations in PM_{10} samples collected at the CROS (c) and GUAR (d) and GUARCRC (e) sites.

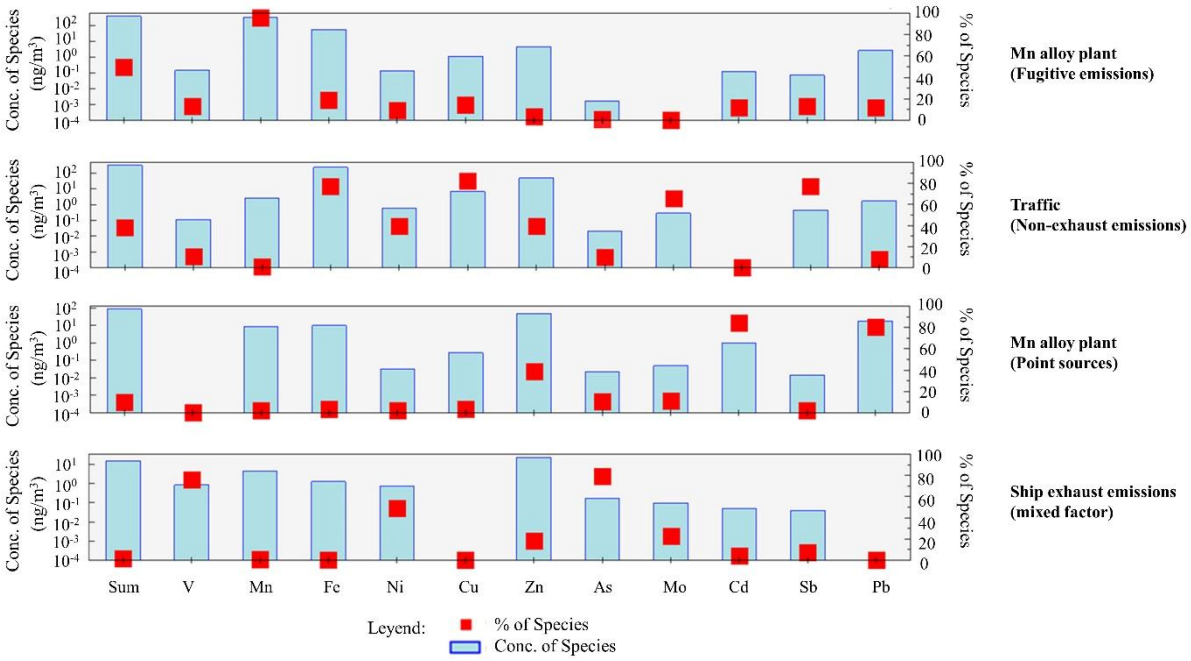

Figure 4. Source profiles of the four factors obtained by PMF at the studied sites.

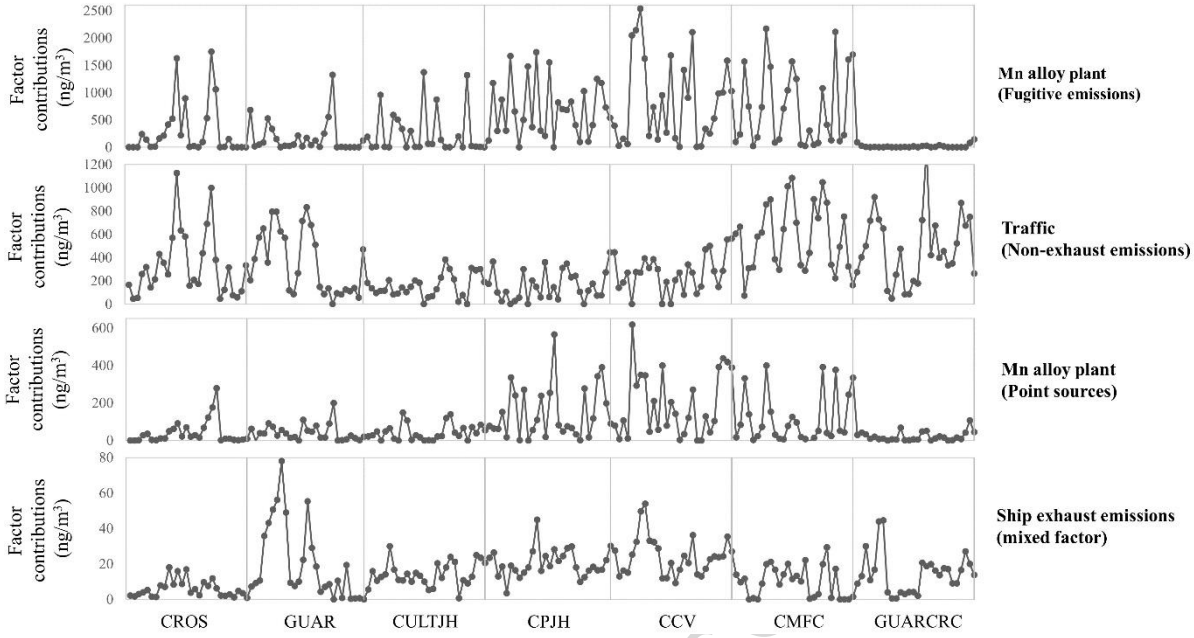

Figure 5. Time series of the factor contributions obtained by PMF at the studied sites.

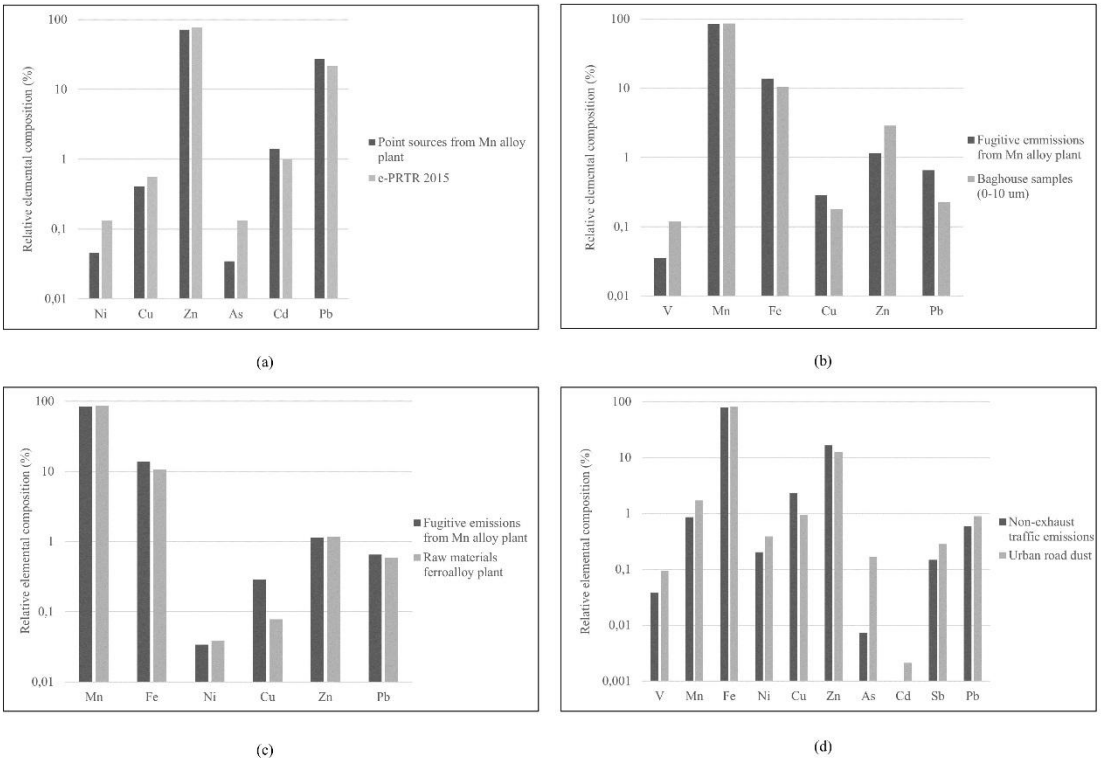

Figure 6. Comparison between the factor profiles from PMF and the calculated factor profiles from identified factors: (a) Point source emissions from the manganese alloy plant located in the area of study, reported in the e-PRTR 2015; (b) Baghouse samples from a manganese alloy plant (0-10 µm). Source: EPA Speciate 4.5 (profile 2840110); (c) Raw materials mixing from a manganese alloy plant (Gunst et al., 2000); (d) Resuspended PM_{10} road dust from an urban-traffic area in Italy, reported by Cesari et al. (2012). Source: Specieurope database v2.0.

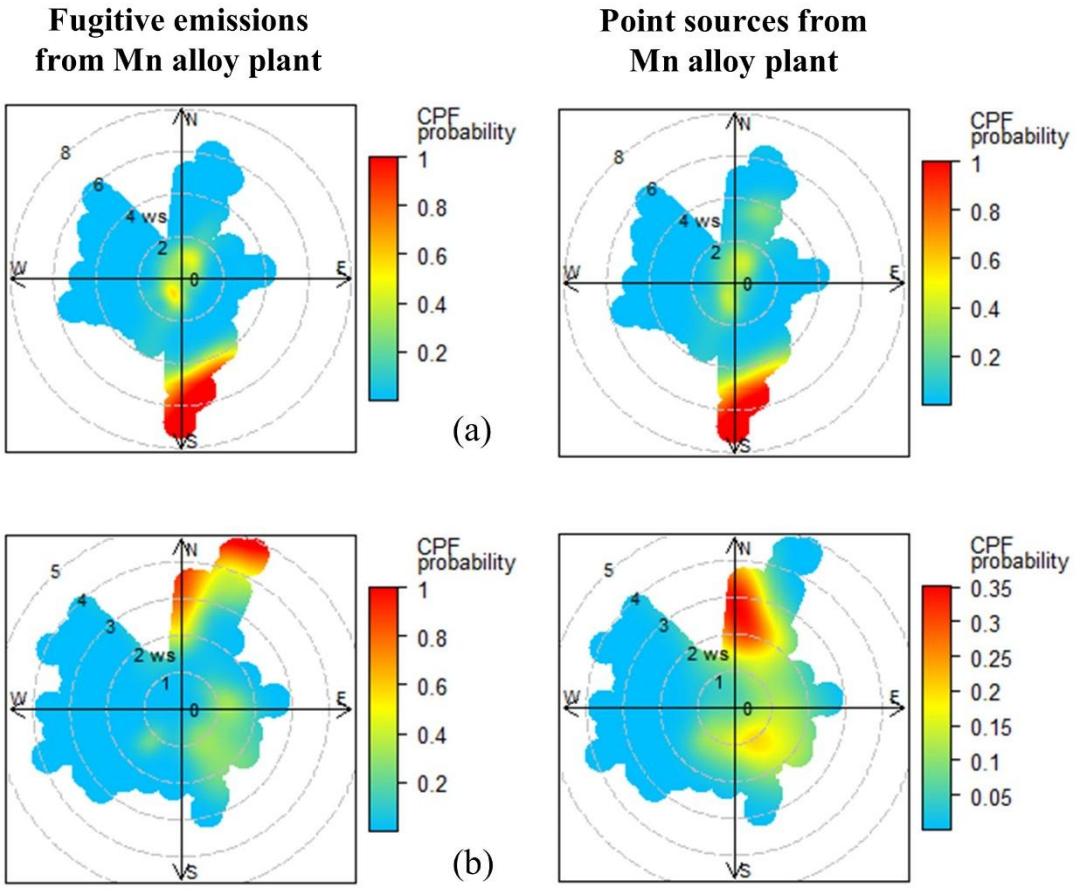

Figure 7. Comparison of the CBPF plots for the 75th percentile of the contributions of the factor profiles associated with the fugitive and point-source emissions from the manganese alloy plant at the nearest receptor sites where samples were collected during the cold period: CROS (a), GUAR (b). Ws: Wind speed (m/s)

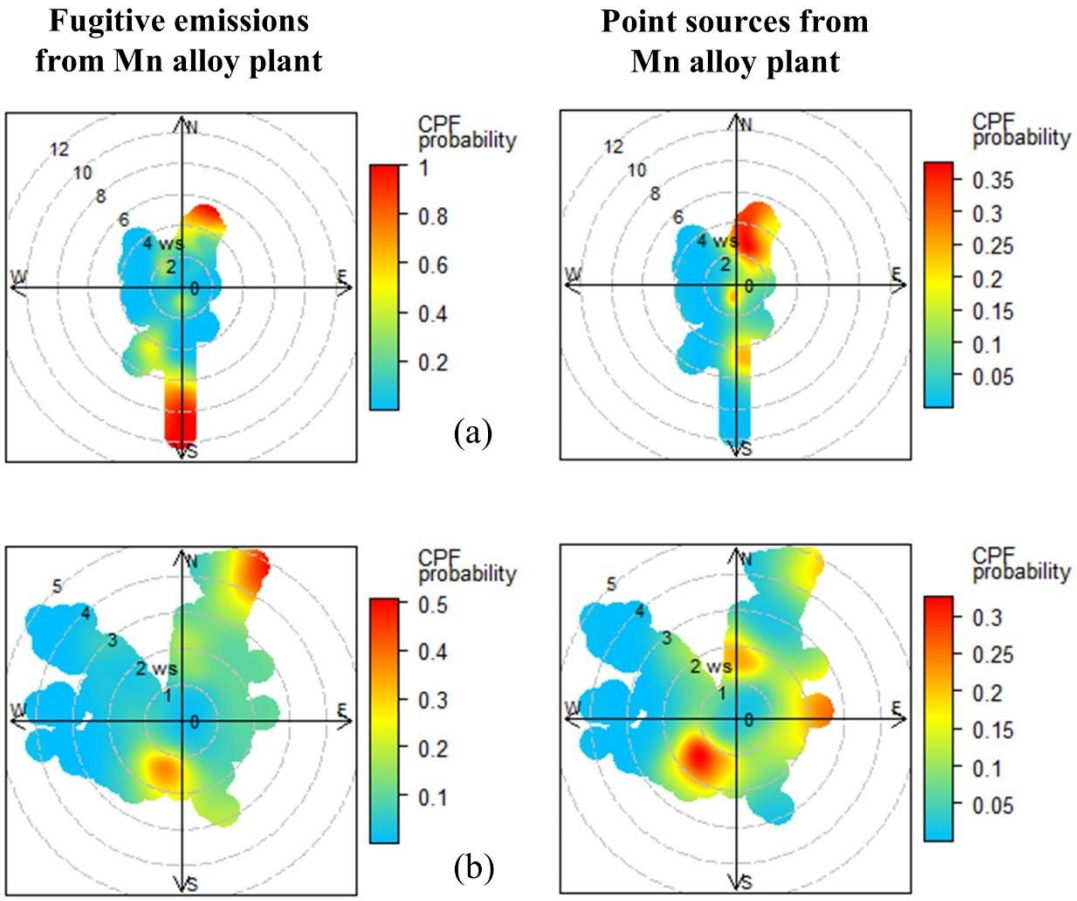

Figure 8. Comparison of the CBPF plots for the 75th percentile of the contributions of the factor profiles associated with the fugitive and point-source emissions from the manganese alloy plant at the nearest receptor sites where samples were collected during the warm period: CCV (a), CPJH (b). Ws: Wind speed (m/s)

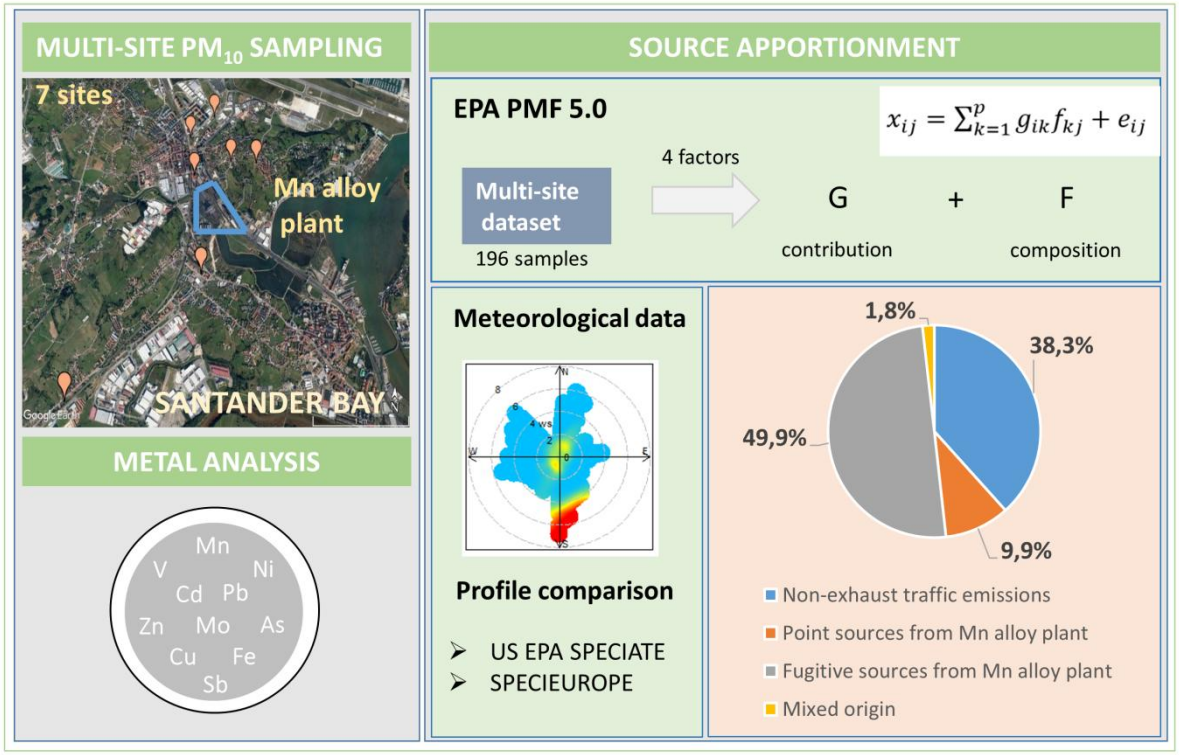

Graphical abstract

Highlights

- A multi-site PM_{10} sampling campaign was developed in an urban/industrial mixed area
- Positive Matrix Factorization (PMF) was used to identify the main metal(loid) sources
- 60% of the total metal(loid) concentrations sourced from a manganese alloy plant
- The PMF analysis differentiated between two emission sources from the manganese alloy plant
- Fugitive emissions accounted for 80% of the total manganese alloy plant emissions

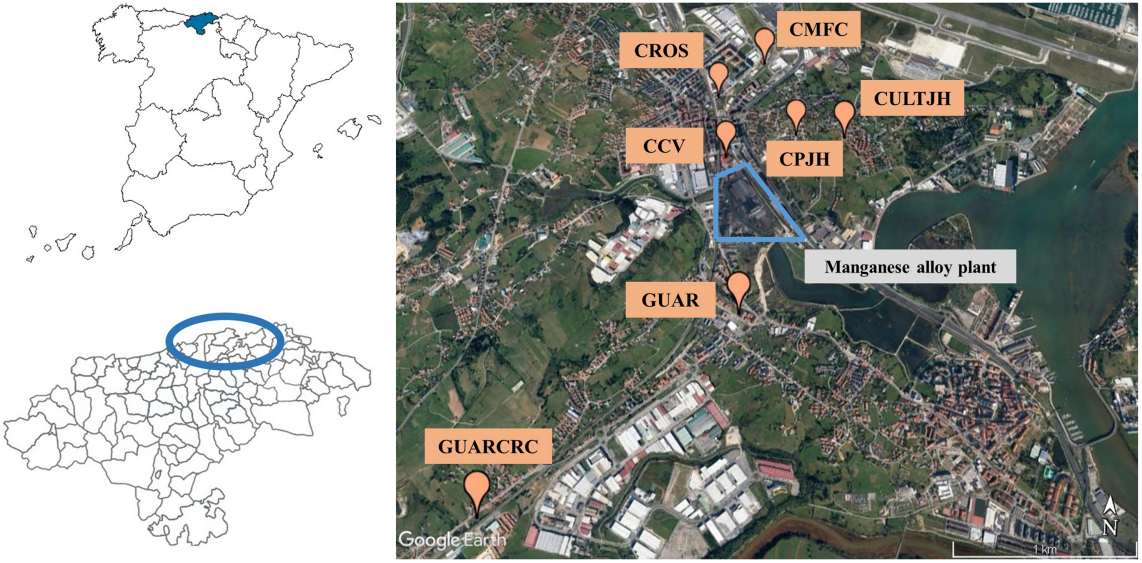
CROS
CMFC
CULTJH
CCV
CPJH
Manganese alloy plant
GUAR
GUARCRC
Google Earth
1 km
N

Figure 1

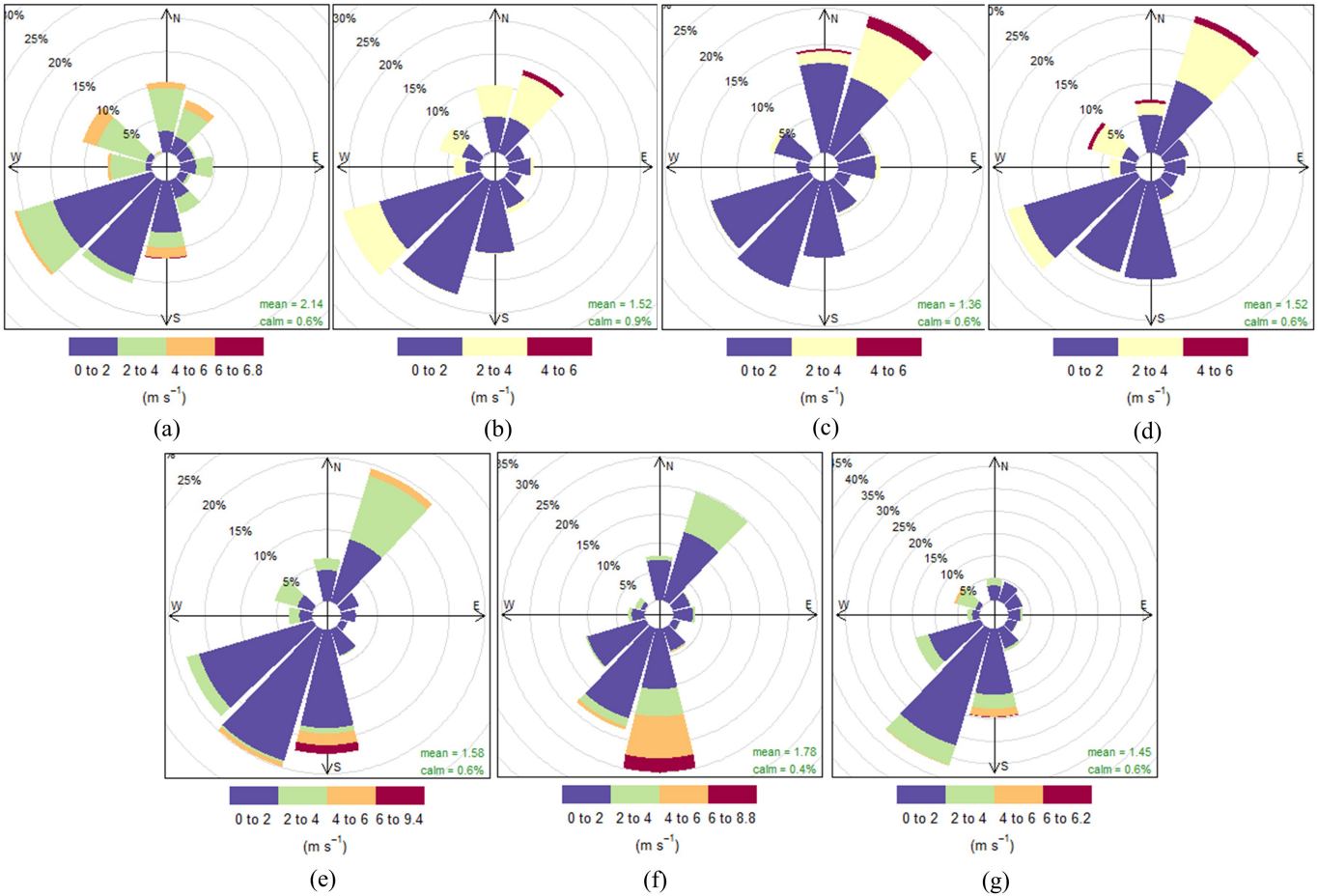
N
E
S
W
mean = 2.14
calm = 0.6%
0 to 2
2 to 4
4 to 6
6 to 6.8
(m s-1)
(a)
mean = 1.52
calm = 0.9%
0 to 2
2 to 4
4 to 6
(m s-1)
(b)
mean = 1.36
calm = 0.6%
0 to 2
2 to 4
4 to 6
(m s-1)
(c)
mean = 1.52
calm = 0.6%
0 to 2
2 to 4
4 to 6
(m s-1)
(d)
mean = 1.58
calm = 0.6%
0 to 2
2 to 4
4 to 6
6 to 9.4
(m s-1)
(e)
mean = 1.78
calm = 0.4%
0 to 2
2 to 4
4 to 6
6 to 8.8
(m s-1)
(f)
mean = 1.45
calm = 0.6%
0 to 2
2 to 4
4 to 6
6 to 6.2
(m s-1)
(g)

Figure 2

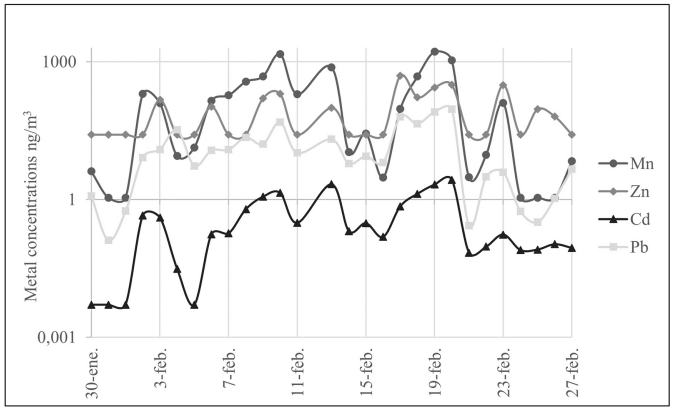

(a)

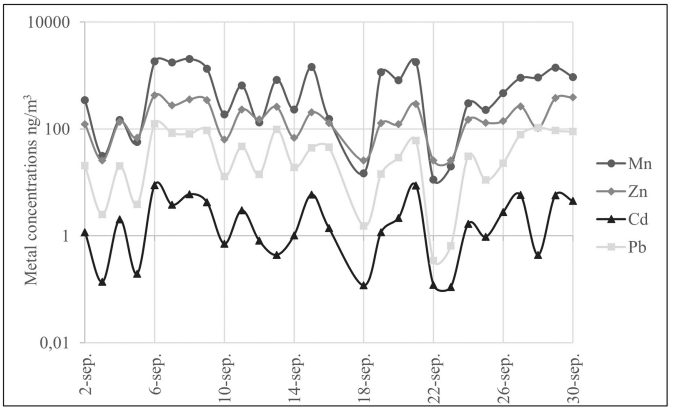

(b)

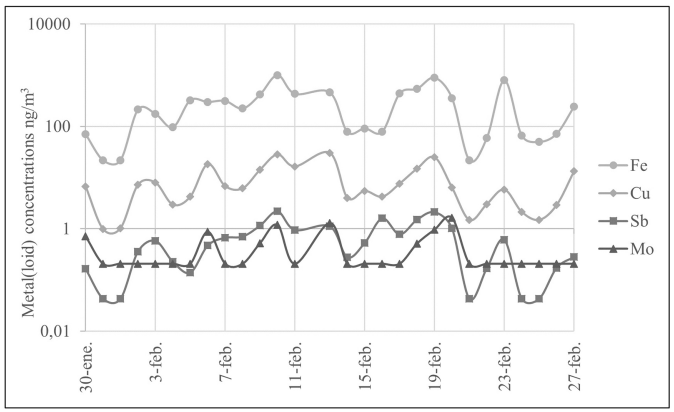

(c)

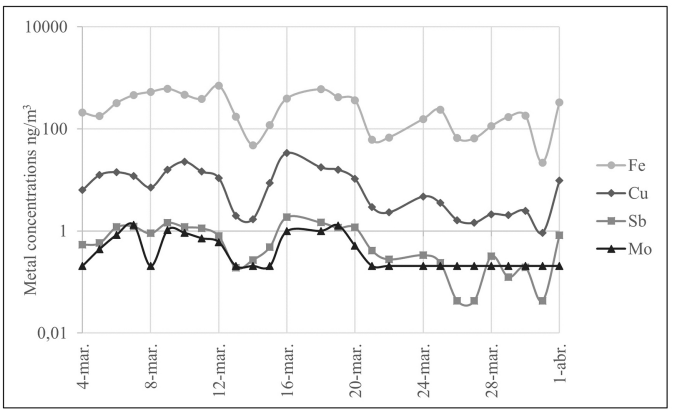

(d)

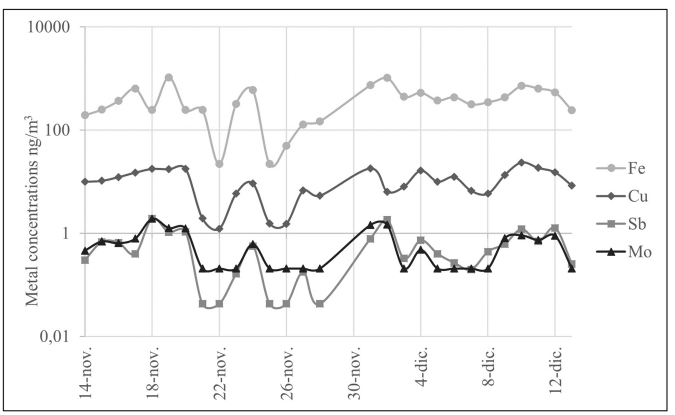

(e)

Figure 3

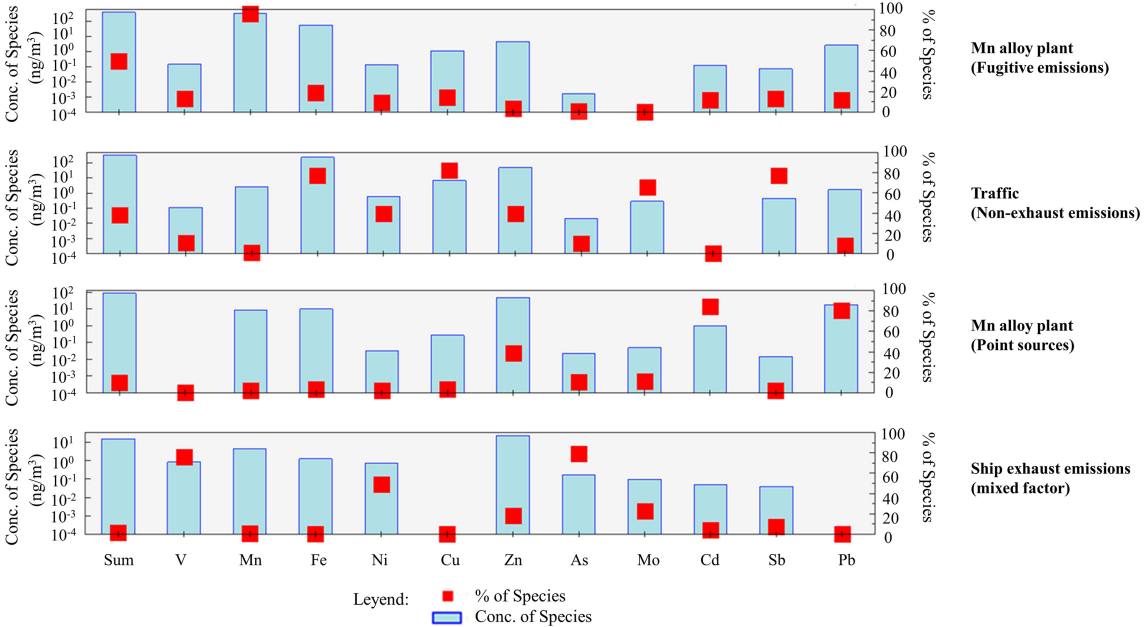
Conc. of Species (ng/m³)
% of Species
Mn alloy plant (Fugitive emissions)
Traffic (Non-exhaust emissions)
Mn alloy plant (Point sources)
Ship exhaust emissions (mixed factor)
Sum
V
Mn
Fe
Ni
Cu
Zn
As
Mo
Cd
Sb
Pb
Leyend:
% of Species
Conc. of Species

Figure 4

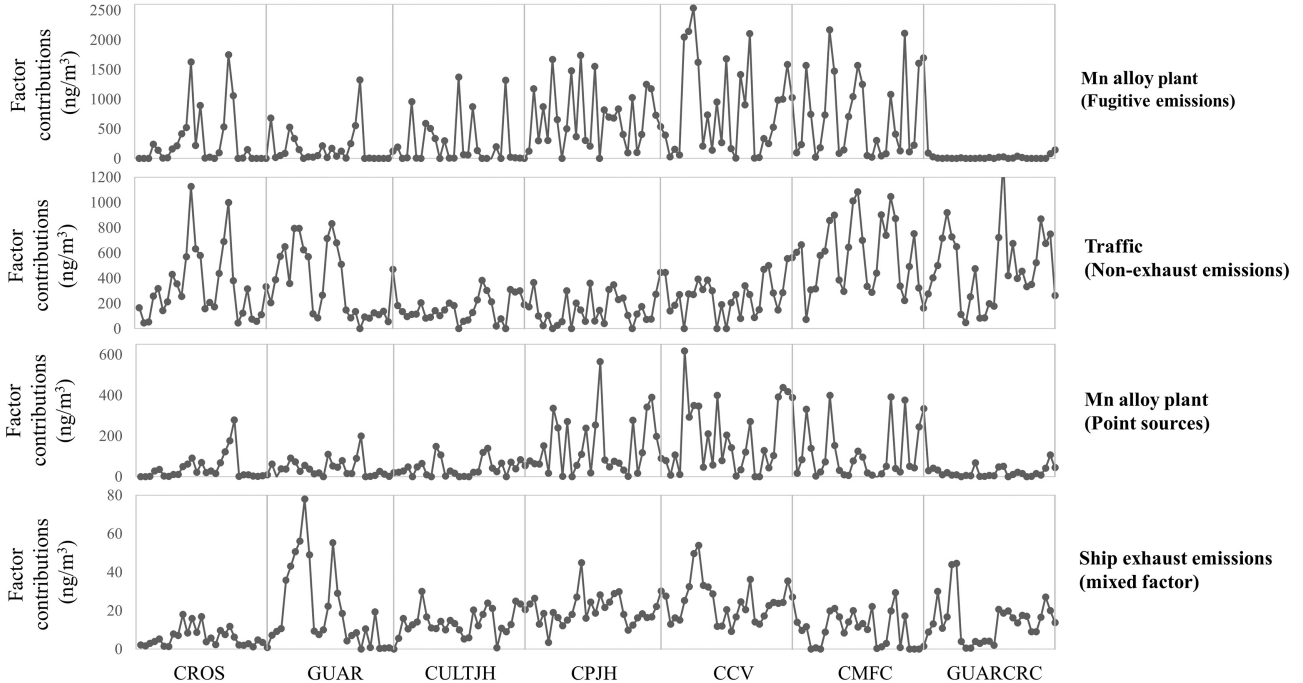
Factor contributions (ng/m3)
2500
2000
1500
1000
500
0
Mn alloy plant (Fugitive emissions)
Factor contributions (ng/m3)
1200
1000
800
600
400
200
0
Traffic (Non-exhaust emissions)
Factor contributions (ng/m3)
600
400
200
0
Mn alloy plant (Point sources)
Factor contributions (ng/m3)
80
60
40
20
0
Ship exhaust emissions (mixed factor)
CROS
GUAR
CULTJH
CPJH
CCV
CMFC
GUARCRC

Figure 5

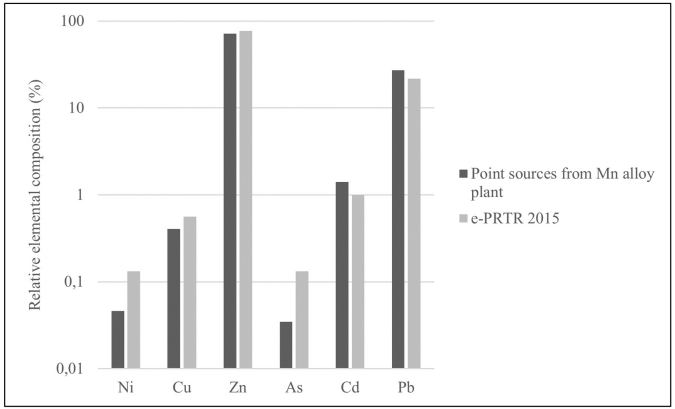

(a)

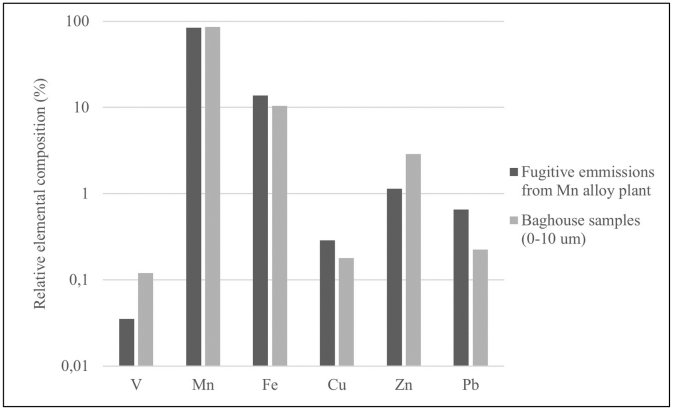

(b)

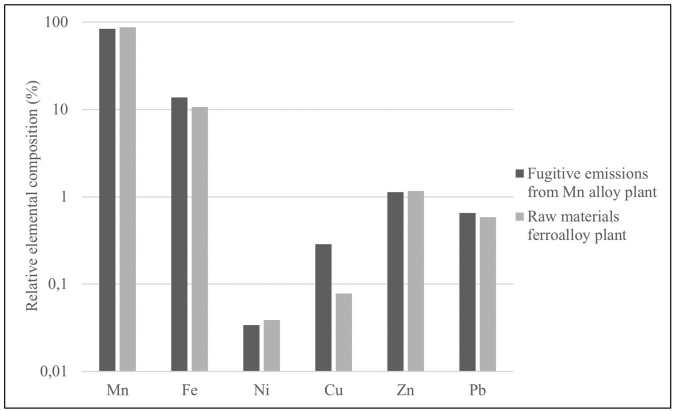

(c)

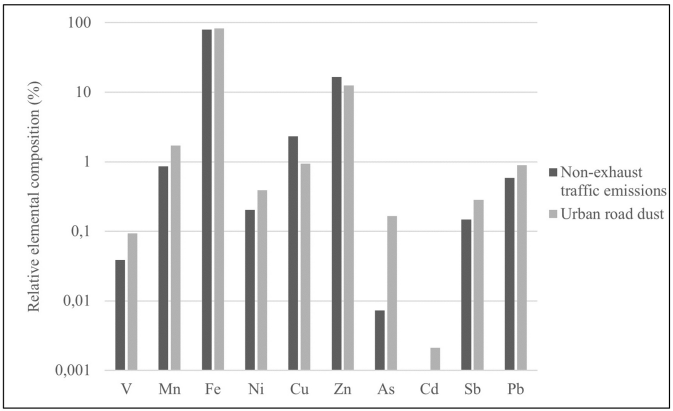

(d)

Figure 6

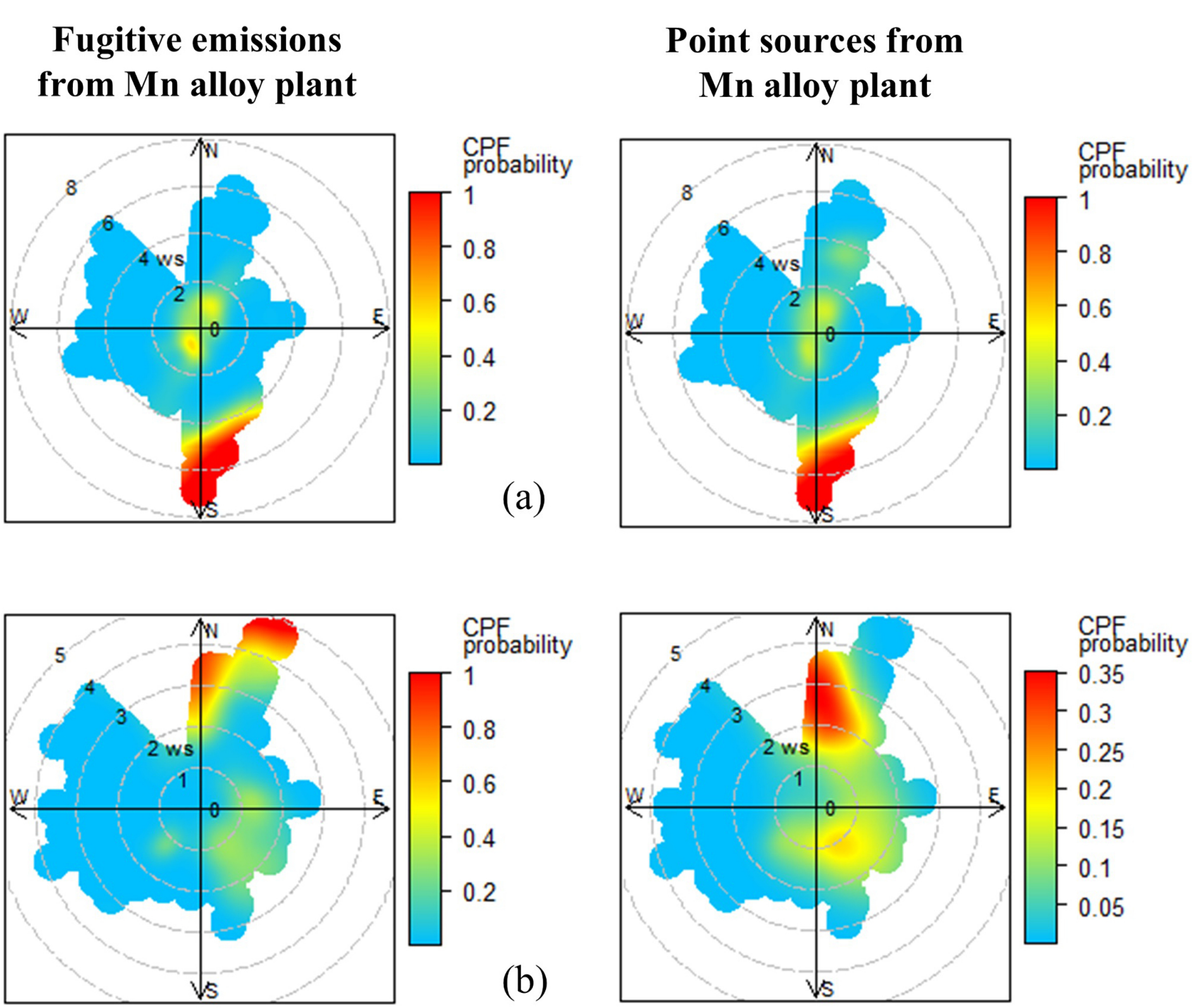
Fugitive emissions from Mn alloy plant
Point sources from Mn alloy plant
N
E
S
W
4 ws
2 ws
CPF probability
1
0.8
0.6
0.4
0.2
0.35
0.3
0.25
0.15
0.1
0.05
(a)
(b)

Figure 7

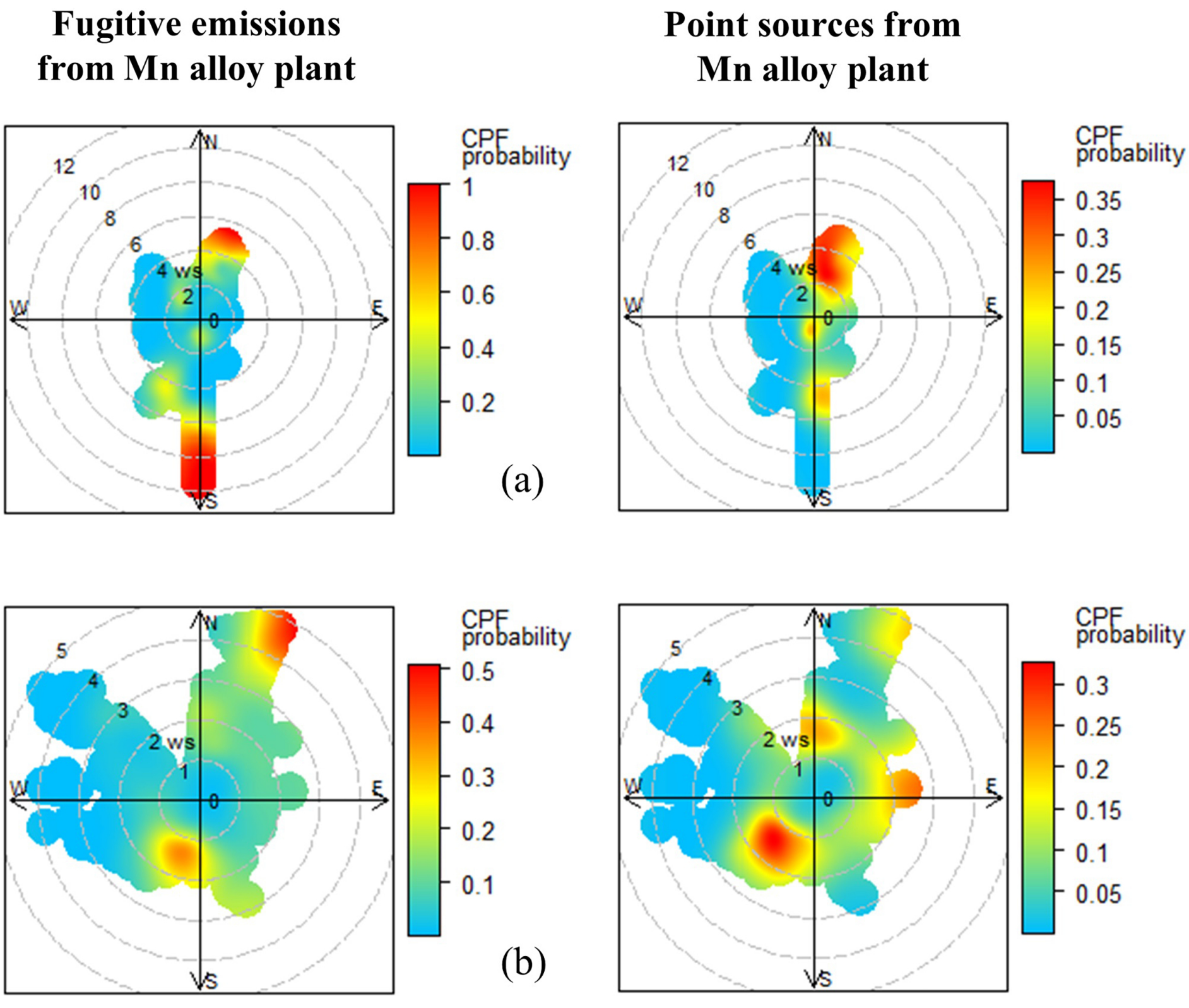
Fugitive emissions from Mn alloy plant
Point sources from Mn alloy plant
CPF probability
1
0.8
0.6
0.4
0.2
0.35
0.3
0.25
0.15
0.1
0.05
0.5
N
E
S
W
12
10
8
6
4 ws
2
0
5
3
2 ws
1
(a)
(b)

Figure 8